Ultrasonic Phased Array Device For Acoustic Imaging In Air

by
Sevan Harput

Submitted to the Graduate School of Engineering and Natural Sciences
in partial fulfillment of
the requirements for the degree of
Master of Science

Sabancı University
August 2007

Ultrasonic Phased Array Device For Acoustic Imaging In Air

APPROVED BY

Assist. Prof. Dr. AYHAN BOZKURT .....
(Thesis Supervisor)

Assist. Prof. Dr. AHMET ONAT .....

Assist. Prof. Dr. HAKAN ERDOĞAN .....

Assoc. Prof. Dr. İBRAHİM TEKİN .....

Assoc. Prof. Dr. MERİÇ ÖZCAN .....

DATE OF APPROVAL: .....

to all Electrical and Electronics Engineers

&

who interested in Acoustics

Acknowledgments

I have been studying in Sabancı University since 2000. I have learnt a lot within these seven years and gained many experience as a microelectronic engineer. The professors of microelectronics group in Sabancı University deserve a special thank. I want to thank all of my professors for their support and teachings.

First, I would like to express my appreciation to my thesis supervisor Assist. Prof. Ayhan Bozkurt for advising me in this thesis work. He guided me both as a mentor and as an academician. Moreover, I am very grateful to my professors Meriç Özcan and İbrahim Tekin for their useful comments and eagerness to help. They provided very necessary feedback on this work and broadened my perspective with their constructive ideas. Additionally, I would like to thank Prof. Mustafa Karaman form Işık University, for sharing his ultrasound knowledge with me. He also helped me while choosing my thesis topic. I am thankful to my thesis defense committee members; Assist. Prof. Ayhan Bozkurt, Assist. Prof. Ahmet Onat, Assist. Prof. Hakan Erdoğan, Assoc. Prof. İbrahim Tekin, Assoc. Prof. Meriç Özcan and Assoc. Prof. Yaşar Gürbüz for their comments and presences.

I would also like to thank people who have contributed in this thesis. Our Lab. Technician Bülent Köroğlu and my friend Yalçın Yamaner have spent many hours with me and helped me while constructing the ultrasonic phased array device. Erman Engin has helped me too much while implementing FDTD method in Matlab. Many thanks to my great colleagues, who always kept my motivation high, and my friends for refreshing my mana. I want to show my appreciation for their endless support and patience.

During my master study, I was supported by the scholarships supplied by Sabancı University and TÜBİTAK. I am grateful to these foundations for enabling the education of many young people like me.

Finally and most importantly, I would like to express my deepest gratitude to my respected and most beloved family who gave me a chance to pursue my ambitions and career and always supported, encouraged and loved me. Thank you with all my heart.

Ultrasonic Phased Array Device For Acoustic Imaging In Air

Sevan Harput

EECS, M.Sc. Thesis, 2007

Thesis Supervisor: Ayhan Bozkurt

Keywords: phased arrays, acoustic imaging, object detection, ultrasound, FDTD

Abstract

The acoustic imaging technology is widely used for medical purposes and underwater imaging. In this work, an ultrasonic phased array device is developed by using piezoelectric transducers to provide autonomous navigation for robots and mobility aid for visually impaired people. To perform acoustic imaging, two different linear transducer arrays are composed with phase-delay focusing phenomenon in order to detect proximate objects with no mechanical scanning.

The requirement of half wavelength spacing can not be satisfied between elements, because of using general purpose transducers. The transmitter array is formed by aligning the transducers with minimum spacing between them, which is 2.11 times of the wavelength. This placement strategy leads to the occurrence of unwanted grating lobes in the array response. To eliminate these grating lobes, the receiver array is formed with a different spacing between each transducer. By forming the receiver array and the transmitter array non-identical, the directivity pattern for both arrays become different. The off-alignment between two arrays causes the grating lobes to appear at different places. Since the overall gain of the system is the product of receiver gain and transmitter gain, the grating lobes diminish for the overall system.

The developed phased array device can transmit/receive ultrasonic waves to/from the arbitrary front directions using electronic sector scanning circuits. A detailed scan can be performed to detect the presence of an object or distinguish different objects.

Havada Akustik Görüntüleme İçin Ultrasonik Faz Dizisi Aygıtı

Sevan Harput

EECS, Master Tezi, 2007

Tez Danışmanı: Ayhan Bozkurt

Anahtar Kelimeler: faz dizisi, akustik görüntüleme, nesne sezim, sesüstü

Özet

Akustik görüntüleme teknolojisi tıbbi amaçlar ve su altı görüntüleme için yaygın olarak kullanılmaktadır. Bu çalışmada, robotlar için özerk dolaşma ve görme engelli insanlar için yer değişim yardımı sağlamak amacıyla piezoelektrik dönüştürücüler kullanılarak bir ultrasonik faz dizisi aygıtı geliştirildi. Mekanik tarama yapmadan yakın nesneleri saptamak amacı ile faz gecikmesi sayesinde odaklama fenomeni kullanılarak akustik görüntüleme yapmak için iki farklı doğrusal dönüştürücü dizisi oluşturuldu.

Dizi elemanları arasındaki yarım dalga boyu aralığı gereksinimi genel amaçlı dönüştürücüler kullanıldığı için karşılanamamıştır. Verici dizisi, dönüştürücüler arasında en az boşluk olacak şekilde sıralanarak oluşturuldu: dalga boyunun 2.11 katı. Bu yerleştirme stratejisi, dizi tepkisinde istenmeyen yan loblar oluşmasına sebep oldu. Bu istenmeyen yan lobları ortadan kaldırmak için alıcı dizisi dönüştürücüler arasında farklı bir aralıkla bırakılarak oluşturuldu. Alıcı ve verici dizileri özdeş olmayacak şekilde oluşturularak, iki dizi için de yönelme örüntüsünün farklı olması sağlandı. Sistemin kazancı alıcı kazancı ve verici kazancının çarpımından oluştuğundan dolayı, yan loblar tüm sistem için azaldı.

Geliştirilen faz dizisi aygıtı, elektronik sektör tarama devresini kullanarak istenilen yönlerde/yönlerden ultrasonik dalgalar gönderebilir/alabilir. Bu sayede, varolan nesneleri bulmak ve farklı nesneleri birbirinden ayrımak için detaylı tarama yapılabilir.

Table of Contents

Acknowledgments v

Abstract vi

Ozet vii

1 Introduction 1
- 1.1 Phased Array Acoustic Imaging . . . 2
- 1.2 Motivation . . . 4
  - 1.2.1 Predeveloped Devices . . . 4
  - 1.2.2 Methodologies based on human-robot interactions . . . 6

2 Phased Arrays 9
- 2.1 Linear Phased Arrays and Array Factor . . . 10
- 2.2 Ranging Method and Scanning Technique . . . 14

3 The Finite-Difference Time-Domain Method 16
- 3.1 Derivation of Acoustic FDTD Equations . . . 17
- 3.2 Implementation of FDTD in Matlab Code . . . 20

4 Design of the Acoustic Phased Array System/Device 25
- 4.1 Transducer Selection . . . 26
- 4.2 Ultrasonic Phased Array Design and Design Parameters . . . 28
  - 4.2.1 Placement Strategy . . . 30
- 4.3 Design of Driver and Readout Circuits . . . 33
  - 4.3.1 Pulse Generation and Driver Circuitry . . . 34
  - 4.3.2 Pulsing and Receiving with Microcontroller . . . 37

5 Experiments 39
- 5.1 Gain Measurements . . . 39
  - 5.1.1 Directivity Pattern of Single Transducer . . . 40
  - 5.1.2 Directivity Pattern of Transmitter Array . . . 41
  - 5.1.3 Directivity Pattern of Receiver Array . . . 42
- 5.2 Experiments . . . 43

5.2.1 Experiment I 44
5.2.2 Experiment II 49
5.2.3 Experiment III 50
5.2.4 Experiment IV 51
5.2.5 Experiment V 52
5.2.6 Experiment VI 53
5.2.7 Experiment VII 54

6 Conclusions **55**
6.1 Error Factors 56
6.1.1 Frequency Errors 56
6.1.2 Phase Errors 57
6.1.3 Placement Errors 58

Bibliography **59**

Appendix **63**

A Directivity Patterns For Different Angles **63**

B Receive Beam Forming **75**

List of Figures

2.1 Two element array 10
2.2 Two element array far-field observation 11
2.3 N element array with uniform geometry 12

3.1 (a) Transducer with the real dimensions, (b) Transducer modified for desired directivity pattern 21
3.2 Bitmap input file for Matlab code 22
3.3 Simulation result for the input at Figure 3.2 23
3.4 Phased array simulation (array is focused to 5°) 24

4.1 Polaroid transducer, SRF04 Transducer, Off-the-shelf Transducer with unknown specifications(respectively) 27
4.2 Radiation pattern of Transmitter array 30
4.3 Gain of Receiver array 32
4.4 Gain of overall system (TX × RX) 32
4.5 Receiver and transmitter array 33
4.6 Object placed with an angle of θ and distance of r 34
4.7 Pulse generation 35
4.8 Powerful Driver circuitry 35
4.9 Driver circuitry 36
4.10 Pulse generation and driver circuitry with microcontroller 37
4.11 Receiver circuitry with microcontroller 38

5.1 Measurement setup 39
5.2 False path from ground 40
5.3 Gain of single transducer 41
5.4 Gain of transmitter array 41

5.5 Gain of receiver array 42
5.6 Gain of receiver array 42
5.7 Experiment-I Setup 44
5.8 Received signal from receiver RX-0 (for $\theta = 0°$) 44
5.9 Received signal from receiver RX-0 (for $\theta = 0°$) 45
5.10 Received signal from receiver RX-0, RX-1 and RX-2 (for $\theta = 0°$) . . . 45
5.11 Received signal from receiver RX-0, RX-1 and RX-2 (for $\theta = 0°$) . . . 46
5.12 Processed signal for $\theta = 0°$ after receive beam forming 46
5.13 Received signal from receiver RX-0, RX-1 and RX-2 (for $\theta = 5°$) . . . 47
5.14 Processed signal for $\theta = 5°$ after receive beam forming 47
5.15 Experiment-I Result 48
5.16 Experiment-II Setup 49
5.17 Experiment-II Result 49
5.18 Experiment-III Setup 50
5.19 Experiment-III Result 50
5.20 Experiment-IV Setup 51
5.21 Experiment-IV Result 51
5.22 Experiment-V Setup 52
5.23 Experiment-V Result 52
5.24 Experiment-VI Setup 53
5.25 Experiment-VI Result 53
5.26 Experiment-VII Setup 54
5.27 Experiment VII Result 54

A.1 Directivity Pattern of Transmitter Array (for 0°) 64
A.2 Directivity Pattern of Receiver Array (for 0°) 64
A.3 Directivity Pattern of Overall System (for 0°) 65
A.4 Directivity Pattern of Transmitter Array (for 2.5°) 65
A.5 Directivity Pattern of Receiver Array (for 2.5°) 66
A.6 Directivity Pattern of Overall System (for 2.5°) 66
A.7 Directivity Pattern of Transmitter Array (for 5°) 67
A.8 Directivity Pattern of Receiver Array (for 5°) 67
A.9 Directivity Pattern of Overall System (for 5°) 68

A.10 Directivity Pattern of Transmitter Array (for 7.5°) 68
A.11 Directivity Pattern of Receiver Array (for 7.5°) 69
A.12 Directivity Pattern of Overall System (for 7.5°) 69
A.13 Directivity Pattern of Transmitter Array (for 10°) 70
A.14 Directivity Pattern of Receiver Array (for 10°) 70
A.15 Directivity Pattern of Overall System (for 10°) 71
A.16 Directivity Pattern of Transmitter Array (for 12.5°) 71
A.17 Directivity Pattern of Receiver Array (for 12.5°) 72
A.18 Directivity Pattern of Overall System (for 12.5°) 72
A.19 Directivity Pattern of Transmitter Array (for 15°) 73
A.20 Directivity Pattern of Receiver Array (for 15°) 73
A.21 Directivity Pattern of Overall System (for 15°) 74

B.1 Received data 76

List of Tables

3.1 Relation between the TM waves and sound waves 18

4.1 Transducer frequency and required speed for microcontroller 26

4.2 Transducer features 28

5.1 Device parameters used in experiments 43

A.1 Phase delays between the array elements 63

Chapter 1

Introduction

The acoustic imaging technology is widely used for medical purposes, underwater imaging and non-destructive-testing applications. In the past few decades acoustic imaging in air become popular with the piezo-ceramic[1] transducers which are matched to air and have a fast time response. By using piezoelectric transducers, an acoustic imaging device is developed to provide autonomous navigation for robots and mobility aid for visually impaired people. Ultrasonic phased arrays are used to perform acoustic imaging in order to detect proximate objects with no mechanical scanning [1]. By combining B-Scan technique and phase-delay focusing phenomenon two different linear transducer arrays are composed of four elements each.

In this work, a device was built with commercially available ultrasonic transducers to detect obstacles on the way within a safety distance. Compactness and low power consumption are important design criteria as the designed device will be carried by the visually impaired person. The device transmits ultrasound beams to different directions at a regular time interval. The emitted ultrasound wave will be reflected back to the receiver array, if any object is present on its way. Both receiver and transmitter arrays work according to phase beam forming principle. By using the device, the distance and location of an obstacle can be detected. The obtained data will be used to give the object's positional information to the user.

The working principle of the device is based on acoustic scanning. The developed phased array device can transmit/receive ultrasonic waves to/from arbitrary directions (15° to -15°) using electronic sector scanning circuits. The angular sam-

[1] *Piezoelectricity* is the property of some ceramic materials and crystals to generate voltage in response to applied sound, or generally mechanical stress. The piezoelectric effect is reversible; by externally applying voltage to piezoelectric materials sound waves can be generated.

pling spacing is 2.5°, which means that the device can direct the output beam to 13 distinct directions from 15° to -15°. Transmitter and receiver array are controlled by a microcontroller, so it is possible to adjust the phase delay between the each elements of the array. By adjusting the phase delays of transducer arrays a detailed scan can be performed in order to detect the presence of the object or to distinguish different objects with a resolution of 1 cm at 0.25 m and 10 cm at 2.5 m. It is obvious that by applying different phase delay schemes it is possible to adjust the phased array device for specific applications.

1.1 Phased Array Acoustic Imaging

In this section the advantages of phased array acoustic imaging will be given. It is preferred to use acoustic techniques rather than the optics and a phased array is formed rather than mechanical scanning. The advantages and disadvantages of the various imaging techniques will be discussed, before starting to describe the phased array acoustic imaging.

Optic vs. Acoustic

There are two widely used imaging techniques; optical and acoustic. They both have advantages over each other for different applications. Although considerable success has been obtained with optical techniques, there are many situations in which acoustic imaging is more appropriate. Examples include lightless and smoky environments, undersea, and objects involving highly polished or transparent surfaces.

In principle both techniques are similar, but acoustics has some advantages over optics in some applications. Optical images map a three dimensional object or a volume into a two dimensional intensity map in a single plane. The positions of objects can be determined by this intensity map, which is in a direction normal to the viewing axis. The range of the object cannot be found from a single image unless some form of structured light is used. However with acoustics three dimensional images can be generated by measuring both range and bearing of targets [2]. Beyond having such an advantage, the usage of acoustic transducers in air is still limited. Acoustics loses its popularity in many cases due to physical restrictions;

slow speed of propagation and high attenuation. However, for short-range applications, like autonomous navigation for robot or other mobile platforms, acoustic imaging is widely used. Since acoustic imaging can provide discrimination between close objects and the background with a cheap, reliable and low power alternative to optical or lidar/radar sensors [3].

After comparing the optics and acoustics, it is decided to use acoustic imaging for this application, which can be interpreted as a short range application. By using ultrasonic transducers an imaging device can be developed, but the structure of the imaging device has to be decided on first.

Mechanical Scan vs. Phased Array

There exists two main methods for scanning a medium line by line to form an image with moving the ultrasonic beam. A single acoustic transducer can be moved mechanically for changing the position the beam, or an array of transducer elements can be electronically controlled to achieve a desired transmit and receive pattern along a line [4].

Mechanical scanning is an approach which reduces the number transducers to be used for acoustic imaging. It is cheaper to use a single transducer, however, this technique is rather slow, and has a poor lateral resolution. Since the electronically controlled beam can be arbitrarily positioned to any given direction, the speed is many times faster than a mechanically controlled system.

In many applications the mechanical scanning is still in use but rather than rotating a single transducer, an electronically controlled phased array would give better results. A phased array requires a large number of transducers for enlarging the aperture size. In many cases, large apertures are needed to overcome diffraction limitations, and to increase the viewing directions [5]. However, the speed is a very crucial in many applications; a successful imaging can be accomplished for real time applications by using phased arrays.

1.2 Motivation

The designed device can be used in a robotic platform or as a mobility aid for visually impaired people. Robots collect information with their sensors, similarly visually impaired people can not see their environment but sense. In both of these applications, the ultrasonic phased array device informs a robot or its user about the obstacles around. The navigation of a robot can be controlled or a user can be guided with this device. Since it is a more dramatic and an important issue, the following parts will be reported in an aspect of a mobility aid for visually impaired people.

Mobility of a visually impaired pedestrian is always a problem, because they also need to travel around just like a sighted. "The ability to navigate spaces independently, safely and efficiently is a combined product of motor, sensory and cognitive skills" [6]. Deficiency of any of these skills causes navigational inability and decreases the quality of life. A visually impaired person can not perform a complete mental mapping of the environment and find the possible paths for navigation. Since, most of the required information for the mental mapping process is obtained by visual channel [7]. For this reason, visually impaired people need to be guided due to lack of this crucial information. Thus lots of devices are developed for a safe navigation of their visually impaired user by using earphones, different tones of audio signals, voice commands, or tactile displays.

1.2.1 Predeveloped Devices

During the last 40 years, hundreds of mobility aid devices have been developed for visually impaired people. Even in 90s, about 30 models of different mobility aid devices designed and some of them were in practical use. The Pathsounder [8], Sonic torch [9], Mowat sensor [10], Sonic pathfinder [11] and Nottingham Obstacle Detector [12] are most popular first developed devices. They are also called as obstacle detectors and path indicators, since the user just know that if there is an obstacle in the path ahead or not.

All the specified devices above work with same principle; by sending acoustic waves to detect objects. Sonic torch is a battery operated hand-held device. Similar to sonic torch, Mowat sensor is small hand-held device, where distance of the object

is sent to the user by changing the rate of vibration produced by the device. In contrary, sonic pathfinder is fit on the user's head and sends different tones of audio signal through a headphone.

Based on acoustic, optic or both imaging schemes several electronic travel aid (ETA) devices were introduced, which are mostly focus on improving the mobility of visually impaired people in terms of safety and speed. Acoustic imaging or ultrasound is mostly used for mobility aid devices, including hybrid designs. The optical imaging technique is not widely preferred by the ETA designers. The most popular non-ultrasonic ETA device, which is based on optical triangulation, is"C5 Laser Cane" [13]. It can detect obstacles at head-height by using three laser diodes and three photo diodes as receiver up to a range of 1.5m or 3.5m.

In 1991, the "Ultrasonic Cane" was introduced by Hoydal and Zelano [14]. Developed device uses Polaroid Sensors with its ultrasonic ranging module. The ultrasonic sensors are mounted on a cane and pulsed by a 555 timer chip. The received echo is turned into frequency information with respect to its amplitude by using another 555 timer. The disadvantage of this device is high power consumption and unnecessarily long range, which will be discussed in more detail at Section 4.1.

In 1995, a similar device to ultrasonic cane was introduced by Gao and Chuan [15]. The system, intended to serve as a mobility aid for the blind, consists of four ultrasonic sensors integrated into the cane, and a microcontroller.

In 1997, another electronic travel aid device was introduced by Batarseh, Burcham and McFadyen [16]. This device was designed by using commercially available ultrasonic sensor, the Sona Switch was used to expand the environmental detection range of blind individuals. The sensor is mounted on a lightweight helmet. The result produced by the system is a varying frequency of chirps that is inversely proportional to the distance measured. This is performed by using a monolithic voltage-to-frequency converter, the DC voltage from the sensor is converted into an AC frequency that produces an audible frequency of chirps in two small headphones..

In 1998, the "Smart long lane" was introduced by Cai and Gao [17]. It is based on data fusion of a cane with ultrasonic sensing. The mostly encountered obstacles in the real world environment are categorized as; point, flat surface, and irregular-shaped. The major aim is protection against overhanging obstacles, such as tree

branches or signposts.

In 2002, a pocket PC based system is introduced by Choudhury, Aguerrevere and Barreto [18]. Device consists of a SRF04 ultrasonic range sensors, a digital compass, PIC16 and a counter for measuring the timing. The duration of the echo pulse is measured for range detection. The difference of this product is that it implements a Head Related Transfer Function; used for the synthesis of binaural sound, which can produce in the listener the illusion of a sound that originates at a virtual location around him/her.

In 2004, another device for detecting hanging objects is introduced by Debnath, Hailani, Jamaludin and Aljunid [19]. It uses SRF04 Ranger kit for obstacle detection. The distance of the object is then measured and converted to discrete levels of 1 meter, 2 meters and 3 meters. These discrete levels are then used either to produce three audio signals (with different tones) or three different tactile vibrators.

1.2.2 Methodologies based on human-robot interactions

There are also some other methodologies applied based on human-robot interactions:

In 1984, the "Guide Dog Robot" was introduced by Tachi and Komoriya [20]. The device has a camera and ultrasonic sensors attached to the mobile robot and it works based on automated guided vehicle technology. A navigation map is stored and robots vision system guides the user by adjusting its speed to the users speed.

In 1999, the "Robotic Cane" was introduced by Aigner and McCarragher [21]. The device is based on shared control of robot and the human with two powered wheels and ultrasonic sensors attached to the handle. Each of the sensors has a sweep angle of approximately 20 degree and they detect the presence or absence of obstacles within approximately 1.5m of the cane. All three ultrasonic sensors work independently and an audio warning signal is produced with the outputs of these transducers to alert the user.

In 2001, the "Intelligent Guide-Stick" was developed by Kang, Ho and Moon [22]. It consists of an ultrasound displacement sensor, two DC motors, and a microcontroller. The purpose of the device is to provide a robotic guidance for the visually impaired people. Using an ultrasonic sensor and two encoders, device traces the position of the moving guide stick and determines whether the user moves safely. The

device performs a mechanical scan which makes the ultrasonic sensor turn around the motor axis continuously. Time of flight is used to determine the distance between the sensor and obstacle, where the information is used by a navigation algorithm for path planning.

In 2002, the "Interactive Robotic Cane" was introduced by Shim and Yoon [23]. It consists of a long cane, two steerable wheels and a sensor head attached at the end of handle. The sensor head unit includes of three infrared sensors, ultrasonic sensors and two antennas for contact sensing. This sensor head is placed on a two wheeled steerable axle. Similar to the other canes, user holds this robotic cane in front of him/her while walking. A gyro sensor is placed to the users head to increase human-robot interaction and an earphone is used to alert the user by voice commands.

The most popular devices based on human-robot interactions are "Navbelt" and "Guidecane", both devices are developed in the University of Michigan, Ann Arbor.

In 1994, the "Navbelt" was introduced by Shoval, Borenstein and Koren [13]. The NavBelt consists of a belt equipped with ultrasonic sensors and a small computer worn as a backpack. It is based on obstacle avoidance technologies of mobile robots and warns the user with stereophonic headphones. Navbelt uses an ultrasound sensor array instead of the steering signal and can detect objects in the range of 0.3-10 m. The equipped computer processes the signals arriving from the sensors and applies an obstacle avoidance algorithms. It can work in both guidance and image mode. But this system requires long-period of adaptation even at a low speed.

In 1997, the "GuidCane" was introduced by Borenstein and Ulrich [24]. Similar to the Navbelt, GuidCane uses an array of ultrasound sensors but it is relatively small, light, and easy to use. The working principle is based on a cane steered by user, where a sensor head unit attached at the end of the handle. The GuidCane can apply global path planning when all the environmental information such as positions or shapes of obstacles is known and local path planning for unknown environments. The GuidCane can guide the user around an obstacles with its wheels, user is guided with the movements of the device.

Both devices "Navbelt" and "Guidecane" are optimized and developed in time and become popular [25].

There is currently no phased array device for acoustic imaging in air. The only device uses phased array phenomenon is as ultrasonic obstacle detector introduced by Strakowski, Kosmowski, Kowalik, and Wierzba in 2006 [26]. The developed device only performs receive beam forming with using a single ultrasound source and an array of microphones.

In this chapter, an introduction was given by briefly explaining the phased array acoustic imaging and stating the predeveloped similar devices. Chapter 2 will explain the phased array phenomenon; the formulations and theoretical calculations. This chapter gives a brief information about the theory behind the phased arrays. In Chapter 3 the Finite-Difference-Time-Domain (FDTD) method will be explained first with sound wave equations. After that the implementation of FDTD method in Matlab and the simulation environment will be described. Chapter 4 mentions the important design criteria for the realization process of the phased array device and explains the whole design process. In Chapter 5, the measurements and experiments will be shown. Acoustic imaging is performed for some experimental setups with the developed device, where the functionality of the phased array device is verified by the measurements. Chapter 6 will end to a conclusion by stating the possible future work and error factors.

Chapter 2

Phased Arrays

An acoustic phased array is theoretically the same with the phased array antenna. Phased array antennas consist of a group of antennas in which the relative phases of the respective array elements are varied to change the radiation pattern of the array. The constructive and destructive interference among the signals radiated by the individual antennas determine the effective radiation pattern of the array, which can be reinforced in a desired direction and suppressed in undesired directions [27]. All elements of the phased array are fed with a variable phase or time delay, in order to scan a beam to given angles in space [28].

Similar to the aforementioned phased array structure, an acoustic phased array imaging system basically uses ultrasound waves to detect the objects. Actually, object detection is performed by determining the acoustic reflectivity or opacity of objects in an acoustically transparent medium. The operation of phased array imaging system is depends on focusing the beam to the desired point or angle in space. Varying phase delays are electronically applied between the elements and the resulting beam produces a scan in the image field.

Generally, the phased array technique is a process, which bases on constructive phasal interference of elements controlled by time delayed pulses. The arrays can perform beam sweeping through an angular range, which is also termed as sector scan. Each transducer element of the phased array is usually computer-controlled with software for desired scanning scheme. For controlling the phased array the phase delays of the each element has to be calculated first. The following section will describe the required calculations and formulation of phased arrays.

2.1 Linear Phased Arrays and Array Factor

The simplest array is formed by placing two identical elements along a line. Therefore, to understand array structure better, a two element array will first be considered. Mostly the array principle is explained with the electromagnetics [29], but it is also possible to express it in different ways with referencing to wave equations. The transducer arrays are very similar with the antenna arrays in principle, by replacing the E field with the P(Pressure) an acoustic array can be expressed. This section will explain the array phenomenon according to the acoustic principles.

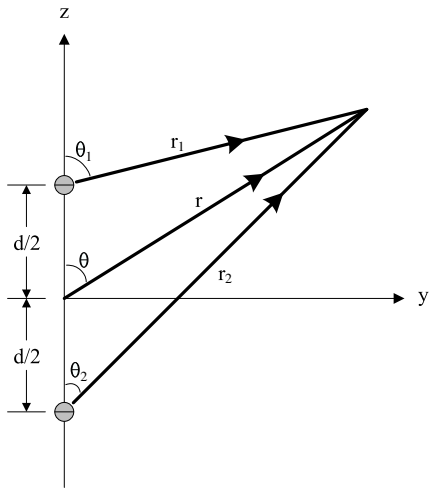

Figure 2.1: Two element array

As shown in Figure 2.1, two acoustic transducers are placed along z-axis. By assuming no coupling between the elements and magnitude of the excitation from both elements are identical, the following equation can be written:

$$P_t = P_1 + P_2 = A\left\{\frac{e^{-j(kr_1-\beta/2)}}{r_1}D(\theta_1) + \frac{e^{-j(kr_2+\beta/2)}}{r_2}D(\theta_2)\right\} \quad (2.1)$$

where P is the pressure, β is the excitation phase difference between the elements, D is the directivity pattern of a single transducer at a specific angle and A is the elemental constant which depends on the excitation amplitude, frequency and properties of the transducer.

The equation 2.1 can be simplified by assuming that the point where the total pressure wanted to be calculated is at the far-field. The far-field observations can

be performed with referring to the Figure 2.2,

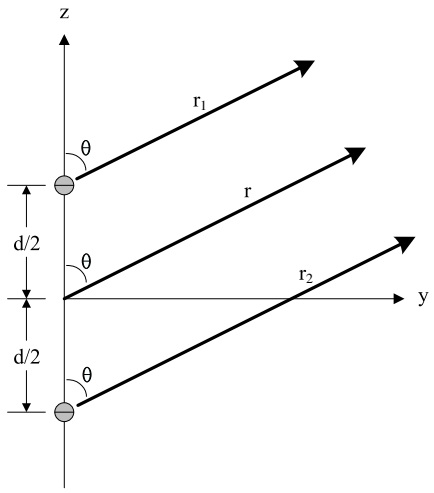

Figure 2.2: Two element array far-field observation

and following assumptions can be done:

$$\text{for amplitude variations} \quad \theta_1 \cong \theta_2 \cong \theta$$

$$r_1 \cong r_2 \cong r \tag{2.2}$$

$$\text{for phase variations} \quad r_1 \cong r - \frac{d}{2}\cos\theta$$

$$r_2 \cong r + \frac{d}{2}\cos\theta \tag{2.3}$$

With considering the far-field assumptions above Equation 2.1 reduce to

$$P_t = \frac{Ae^{-jkr}}{r} D(\theta) \left\{ e^{-j(kd\cos\theta+\beta)/2)} + e^{+j(kd\cos\theta+\beta)/2)} \right\} \tag{2.4}$$

and after some trigonometric simplifications the final equation becomes:

$$P_t = \frac{Ae^{-jkr}}{r} D(\theta) \left\{ 2\cos\left[\frac{1}{2}(kd\cos\theta + \beta) \right] \right\} \tag{2.5}$$

It can be seen from Equation 2.5 that the total pressure through the array is equal to pressure coming from a single element placed at origin multiplied by a factor, which is also called the *Array Factor*.

$$P_t = P(\text{single element at reference point}) \times \text{Array Factor} \tag{2.6}$$

For a two element array of constant excitation amplitude the Array Factor is defined as:

$$AF = 2\cos\left[\frac{1}{2}(kd\cos\theta + \beta) \right] \tag{2.7}$$

The Array Factor is a function of β and d (k depends on characteristic of the elements). The characteristic of the array can be modified by changing the separation between the elements and excitation phase, without changing the elements of the array. In order to change the total pattern of the array, it is not only required to chose a proper element but also geometry of the array and the excitation phase is important. For this reason, Array Factor is mostly used by designers, in the normalized form, to achieve desired array patterns.

$$AF_n = \cos\left[\frac{1}{2}(kd\cos\theta + \beta)\right] \tag{2.8}$$

After introducing the phased array principle with a simple two element array, now it is time to generalize the method for N-element uniform linear array. The uniform array means that all elements have identical amplitudes and spacings between them. Also the succeeding elements must have a progressive phase delay of β, to protect the uniformity of the array.

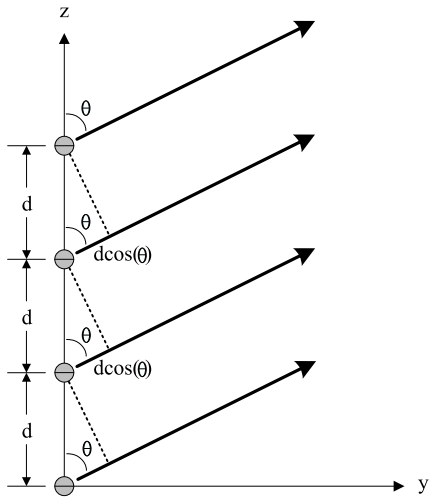

Figure 2.3: N element array with uniform geometry

The Figure 2.3 shows a n element uniform array, where the array factor is calculated by summing the contributions of each element:

$$\begin{aligned} AF &= 1 + e^{+j(kd\cos\theta+\beta)} + e^{+j2(kd\cos\theta+\beta)} + ... + e^{+j(N-1)(kd\cos\theta+\beta)} \\ AF &= \sum_{n=1}^{N} e^{j(n-1)(kd\cos\theta+\beta)} \end{aligned} \tag{2.9}$$

Since the total array factor for a uniform array is the sum of exponentials, the relative phases ψ between the elements has to be selected properly, where the ψ can be used to control the formation and distribution of the array.

$$\begin{aligned} AF &= \sum_{n=1}^{N} e^{j(n-1)\psi} \\ \psi &= kd\cos\theta + \beta \end{aligned} \tag{2.10}$$

After simplifying the equation above by doing the summation, the overall equation reduces to:

$$\begin{aligned} AF &= \left[\frac{e^{jN\psi}-1}{e^{j\psi}-1}\right] = e^{j[(N-1)/2]\psi}\left[\frac{e^{j(N/2)\psi}-e^{-j(N/2)\psi}}{e^{j(1/2)\psi}-e^{-j(1/2)\psi}}\right] \\ &= e^{j[(N-1)/2]\psi}\left[\frac{\sin(\frac{N}{2}\psi)}{\sin(\frac{1}{2}\psi)}\right] \end{aligned} \tag{2.11}$$

If the reference point is set to the physical center of the array, the Array Factor becomes:

$$AF = \frac{\sin\left(\frac{N}{2}\psi\right)}{\sin\left(\frac{1}{2}\psi\right)} \tag{2.12}$$

The maximum value of the Equation 2.12 is equal to N. To achieve a maximum value equal to unity, the Array Factor s usually referred as in normalized form as

$$AF_n = \frac{1}{N}\left[\frac{\sin\left(\frac{N}{2}\psi\right)}{\sin\left(\frac{1}{2}\psi\right)}\right] \tag{2.13}$$

According to the Equation 2.13, the nulls of the array appear at

$$\begin{aligned} \sin\frac{N\psi}{2} = 0 \quad \Rightarrow \quad \frac{N\psi}{2} &= \pm \mathrm{n}\pi \quad , \text{n=1,2,3...} \\ N(kd\cos\theta+\beta) &= \pm 2\mathrm{n}\pi \quad , \text{n}\neq N,2N,3N... \\ \theta_n &= \cos^{-1}\left[\frac{1}{kd}\left(-\beta \pm \frac{2\mathrm{n}\pi}{N}\right)\right] \end{aligned} \tag{2.14}$$

similarly the maximum values occur when

$$\begin{aligned} \frac{\psi}{2} = \frac{kd\cos\theta+\beta}{2} &= \pm \mathrm{m}\pi \quad , \text{m=0,1,2...} \\ \theta_m &= \cos^{-1}\left[\frac{1}{kd}\left(-\beta \pm 2\mathrm{m}\pi\right)\right] \end{aligned} \tag{2.15}$$

For a phased array, the maximum radiation direction can be directed towards the angle θ by equalizing the ψ to zero:

$$\begin{aligned} \psi &= kd\cos\theta + \beta = 0 \\ \beta &= -kd\cos\theta \end{aligned} \tag{2.16}$$

Finally, controlling the progressive phase differences between the identical elements of a uniform array, the radiation can be maximized at a desired point. This is the basic principles of the phased arrays, which are also called scanning arrays. While realizing this phenomenon, the system should be capable of varying these progressive phase differences continuously, in order to perform the electronic scanning operation with a phased array.

2.2 Ranging Method and Scanning Technique

The distance of a target object can be measured in different ways, for instance, pulse-echo, phase measurement or by frequency modulation [2]. The work described here is mostly concerned with pulse-echo method. In a pulse-echo method, to measure both the range (r) and the bearing (θ) of the target, an environmental scan should be proposed. For scanning, it is necessary to use more than one transducer or steer a single transducer mechanically. In sonar and radar applications phased arrays are widely used, because it is easy to change the direction of transmitted beam by varying the phases of different elements. By controlling the relative phase differences between the elements, the environment is scanned electronically. Electronic scan, also termed as electronic raster scan, is performed by sweeping different index points. The same focal law, which requires different phase delays for different scanning angles, is multiplexed across all of array elements; electronic scan is performed at constant angles according to the directivity pattern of the array.

The beam steering applied in this work is based on the described scanning principle above. Beam steering is the ability of a phased array system to electronically sweep the beam through a range of incident angles without physical movement, just changing the direction of the main lobe of radiation pattern. This is widely used in radio transmitters; by changing the phases of the RF signals driving the antenna

elements, the beam steering is accomplished.

The advantage of beam steering is to transmit a pulse whose energy is concentrated in the direction θ. This allows to detect an object at a desired point or to estimate the reflectivity of a point with a distance r and angle θ. To minimize the echoes from reflectors at other locations, the transmitted beam should be steered in the θ direction. For the returning echo, the time delays have to be applied to each signal. When they are summed together the echoes returning from the specified point will add together coherently, whereas echoes from other locations will add destructively.

Chapter 3

The Finite-Difference Time-Domain Method

Modeling an acoustic transducer array is very similar to antenna arrays, which needs a lot of theoretical calculations and computing power. Therefore the simulation method must be chosen wisely. There are several computational electrodynamics modeling techniques which can accurately model an acoustic transducer array, but the Finite-Difference-Time-Domain (FDTD) method is implemented. Because FDTD method is easy to understand and easy to implement in software and it can cover a wide frequency range with a single simulation.

The FDTD method is first introduced by Yee in 1966 [30]. This method is a finite-difference time-marching scheme and it is widely used to solve electromagnetic problems because of its simplicity and effectiveness. It is based on discretization of the differential form of Maxwell's time dependent equations, using central finite difference approximations for the temporal and the spatial derivatives of electric and magnetic fields. Beyond its computational simplicity, the discretization of the Maxwell's equations makes this method computationally very efficient [31]. Since FDTD is performed in the time domain, a broad band response can be obtained with a single simulation. Therefore, electromagnetic problems are solved in a more efficient manner in the time-domain, compared with other methods in the frequency-domain. The most important characteristic of the FDTD method is the adjustment of the grids, which is firstly implemented by Yee [30]. Wave and propagation problems can be solved by using FDTD method, but it needs an infinite FDTD grid. This looks like a very huge problem, but it can be solved easily by implementing Perfectly Matched Layers at the boundaries of your solution space. PML is similar to the walls of anechoic chamber; incident fields are attenuated to zero through

adjusting the conductivities of the solution space at boundaries.

The recent popularity of the FDTD method does not only base on its simplicity and effectiveness, the method is also advanced after Yee. The traditional FDTD has a major drawback; fine geometric details. When high-resolution details compared to the wavelength is necessary, the time step size has to be enormously small in order to achieve constraints specified by stability conditions. Reducing time step size proportionally scales up the number of time steps needed to be executed and increases simulation time. This limitation mostly disappeared by the studies associated with the identification of the correct stability conditions [32], the development of absorbing boundary conditions [33], and the other advancements stated in [34].

3.1 Derivation of Acoustic FDTD Equations

To derive the E field and H field equations, one has to be started with the two well known Maxwell's equations, which are also called as Faraday's law and Ampere's law:

$$\nabla \times E = -\frac{\partial B}{\partial t} - M \tag{3.1}$$

$$\nabla \times H = \frac{\partial D}{\partial t} + J \tag{3.2}$$

And combine them with the medium dependent equations as follows:

$$B = \mu \cdot H \tag{3.3}$$

$$D = \epsilon \cdot E \tag{3.4}$$

$$J = \sigma \cdot E \tag{3.5}$$

$$M = \varsigma \cdot H \tag{3.6}$$

where

E is the electric field [V/m],

H is the magnetic field [A/m],

D is the electric flux density [C/m^2],

B is the magnetic flux density [Wb/m^2],

J is the electric current density [A/m^2],

M is the equivalent magnetic current density [V/m^2],

ϵ is the permittivity of the material [F/m],

μ is the permeability of the material [H/m],

σ is the electric conductivity [S/m],

ς is the equivalent magnetic loss [Ω/m].

By using the equations above, two vector versions of Maxwell's equations are obtained:

$$\nabla \times \vec{E} = -\varsigma \cdot \vec{H} - \mu \cdot \frac{\partial \vec{H}}{\partial t} \tag{3.7}$$

$$\nabla \times \vec{H} = -\sigma \cdot \vec{E} - \epsilon \cdot \frac{\partial \vec{E}}{\partial t} \tag{3.8}$$

The vector components of the curl operators at the equations 3.7 and 3.8 represent a system of three scalar equations for a 2D solution. This can be expressed in Cartesian coordinates as:

$$\frac{\partial E_z}{\partial y} = -\mu \cdot \frac{\partial H_x}{\partial t} \tag{3.9}$$

$$\frac{\partial E_z}{\partial x} = \mu \cdot \frac{\partial H_y}{\partial t} \tag{3.10}$$

$$\frac{\partial H_y}{\partial x} - \frac{\partial H_x}{\partial y} = \epsilon \cdot \frac{\partial E_z}{\partial t} \tag{3.11}$$

After solving the TM waves, the equations are turned into the acoustic equations by using the correspondence between two dimensional sound waves and electromagnetic waves [35]:

TM Waves	Sound Waves
E_z	P
H_x	V_y
H_y	$-V_x$
ϵ	$1/\kappa$
μ	ρ

Table 3.1: Relation between the TM waves and sound waves

where

P is the sound pressure [Pa],

V is the particle velocity [m/sec],

κ is the bulk modulus (stiffness) [N/m^2],

ρ is the density of the material [kg/m^3],

Acoustic equations in a scalar form for a 2D solution can be expressed in Cartesian coordinates as:

$$\frac{\partial P}{\partial y} = -\rho \cdot \frac{\partial V_y}{\partial t} \tag{3.12}$$

$$\frac{\partial P}{\partial x} = -\rho \cdot \frac{\partial V_x}{\partial t} \tag{3.13}$$

$$-\frac{\partial V_x}{\partial x} - \frac{\partial V_y}{\partial y} = \frac{1}{\kappa} \cdot \frac{\partial P}{\partial t} \tag{3.14}$$

Subsequently, the derived acoustic equations are discretized in order to implement the FDTD method, similar to electromagnetic equations. There is only a small difference between them due to the sign differences between the discretized electromagnetic equations and acoustic equations. The TM wave and sound wave equations are mostly matches with each other, because no shear waves are calculated in the equations. The acoustic equations only include the longitudinal waves, which are very similar to electromagnetic waves.

$$V_{x\,i,j+1/2}^{\,n+1/2} = V_{x\,i,j+1/2}^{\,n-1/2} - \frac{\Delta t}{\rho \Delta y}\left[P_{z\,i,j+1}^{\,n} - P_{z\,i,j}^{\,n}\right] \tag{3.15}$$

$$V_{y\,i+1/2,j}^{\,n+1/2} = V_{y\,i+1/2,j}^{\,n-1/2} - \frac{\Delta t}{\rho \Delta x}\left[P_{z\,i+1,j}^{\,n} - P_{z\,i,j}^{\,n}\right] \tag{3.16}$$

$$P_{z\,i,j}^{\,n+1} = P_{z\,i,j}^{\,n} - \frac{\kappa \Delta t}{\Delta x}\left[V_{y\,i+1/2,j}^{\,n+1/2} - V_{y\,i-1/2,j}^{\,n+1/2}\right] - \frac{\kappa \Delta t}{\Delta y}\left[V_{x\,i,j+1/2}^{\,n+1/2} - V_{x\,i,j-1/2}^{\,n+1/2}\right] \tag{3.17}$$

To solve the discritized acoustic waves above, they are iterated in every time step. First, it is used the first two equations to compute the V_x and V_y at the n+1/2 time step from P at the time step n. Then the last equation is used to compute P at time step n+1. Alternating between these two steps, the solution is propagating forward in time.

Finally, after implementing the FDTD method in practice, it is needed to add sources, apply boundary conditions, provide the stability conditions, and meet some

other requirements on the field solutions to obtain correct results from the simulations.

3.2 Implementation of FDTD in Matlab Code

By deriving the discretized acoustic equations and defining a simulation space, the implementation of FDTD method is finished. But the artificially labeled boundaries at the edges of the simulation space have to be turned into absorbing layers to prevent the interference between propagating waves and the reflections at boundaries. Perfectly Matched Layers are implemented as in the [36]; symmetric in x and y directions and modified time constants to include exponential difference time advance. But the Matlab code adds the PMLs next to the outermost regions of the given medium. There is also another alternative like turning the outermost regions of the given medium into PMLs, but this causes problems when a non-host material is defined in the outermost region. For this reason, rather than implementing absorbing boundaries, perfectly matched layers are added next to the outermost regions. The number of PML can be set by modifying a variable.

Beyond discretizing the acoustic equations and defining the absorbing boundary conditions, the other important criterion is numerical stability. In FTDT method, finite difference wave equations have a well known stability condition called *Courant condition* [35, 36]. According to the Courant stability condition the normalized time differences $\Delta u = c_0.\Delta t$ and the spatial differences Δx and Δy has to be chosen according to the normalized material parameters:

$$\frac{\Delta u}{\Delta x} = \frac{\Delta u}{\Delta y} < \frac{1}{\sqrt{2}.\max(\overline{\kappa}, \underline{\rho})} , \tag{3.18}$$

where normalized material parameters are $\underline{\rho} = \rho_0/\rho$ and $\overline{\kappa} = \kappa/\kappa_0$.

Courant condition increases the number of requirements to be met and brings difficult restrictions to numerical analysis of wave propagation in the simulation [35]. The normalized material parameters $\underline{\rho}$ and $\overline{\kappa}$ are extremely larger than unity in this case, where they must be less than or equal to the unity to reach the stability. For instance, an aluminum object in air has a parameter contrast of 7×10^5. In order to met the Courant condition the time steps size can be decreased by 10^6, but it turns

out in an extremely large amount of computational steps. In order to increase the time step size and reduce the simulation time, it is decided to change the material parameters. Since acoustic wave propagation into the targets is not important for object detection, the Courant stability condition is reached by modifying the ρ and κ of the target materials [35]. The reflections from the target objects stay same, but the speed of the acoustic wave is changed in the material. By dividing the κ with 10^6 and multiplying the ρ with 10^6 the Courant stability condition is reached and the acoustic impedances stay same, since $\rho \times \kappa$ product does not change.

Inserting the environmental data and dimensions of the solution space is the last step of the simulation. The easiest way of specifying the sources, transmitters and reflectors is creating an image file. The Matlab code gets input from a bitmap image. It reads the image according to its color code and detects if the drawn figure is source, receiver, or some kind of object. Bitmap image includes 8 bit RGB data, which means that just looking at the data coming from the red 253 different objects can be identified. Since one color is reserved for propagation medium, one for source and one for receiver.

While preparing the input image file, the transducers are measured and drawn with the same dimensions. By setting Δx and Δy to 0.2 mm independent to working frequency, it is easy to compose a bitmap image of transducers for every simulation. Drawings of the transducers can be seen in the Figure 3.1. White area in the figure is the active area of the transducer, which is perceived as source. The gray parts are the aluminum cage of the transducer.

(a) (b)

Figure 3.1: (a) Transducer with the real dimensions, (b) Transducer modified for desired directivity pattern

Directivity patterns of ultrasonic transducers are taken into account while drawing their equivalent images. In the drawing the piezoelectric material inside the transducer and its cage is drawn, since one of them transmits the sound waves and the cage shapes the directivity pattern. First image is formed with the exact dimensions of real transducer (Figure 3.1.a), and then the directivity pattern of the sketched transducer is measured within the simulation. It is seen that the radiation pattern of the real transducer and the transducer in the simulation do not match, so it is decided to modify the transducers. A new input file is formed by changing the shape of the aluminum cage (Figure 3.1.b), which changes the directivity pattern of drawn transducer in the simulations. Finally, the same directivity pattern with a real transducer is achieved.

After drawing a single transducer and verifying its directivity patter, the transmitter array can be formed. A complete drawing of an input file can be seen from the figure below, Figure 3.2. The transducer array is formed with 4 elements and an object is placed in front of the transmitter array (The material coefficients of the reflector objects are changed as stated above in order to achieve the Courant's stability condition). The Matlab code understands the aluminum cage of the transducer and target object by checking their color codes.

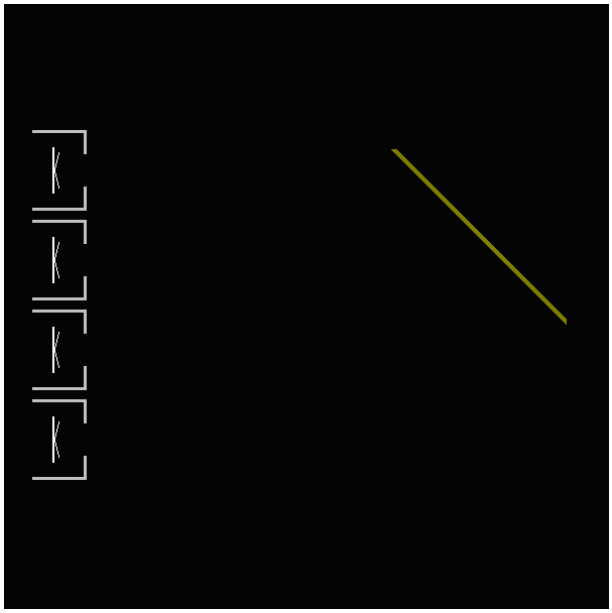

Figure 3.2: Bitmap input file for Matlab code

The simulation results can be evaluated by looking at the plots at predetermined time steps or checking the saved data after the simulation. Because of the time step is set to 88 ns; the simulation takes too much time for the objects placed at long distances. For instance, if the object is placed at 2 meter far from the transmitters, the number of iteration cycles is 132000. For this reason, the simulation is recorded as a movie and the results are evaluated later. It is also possible to save the simulation results by defining a pixel or pixels as receiver and saving the data at that point, and then the echo reflecting back from the object can be analyzed.

In this case, a simulation is done with the input at Figure 3.2. The propagating sound waves and the reflected echoes can be seen at a predetermined time steps as in Figure 3.3. The simulation environment is 0.12 meter by 0.12 meter and there is a brass reflector in front of the transducer array.

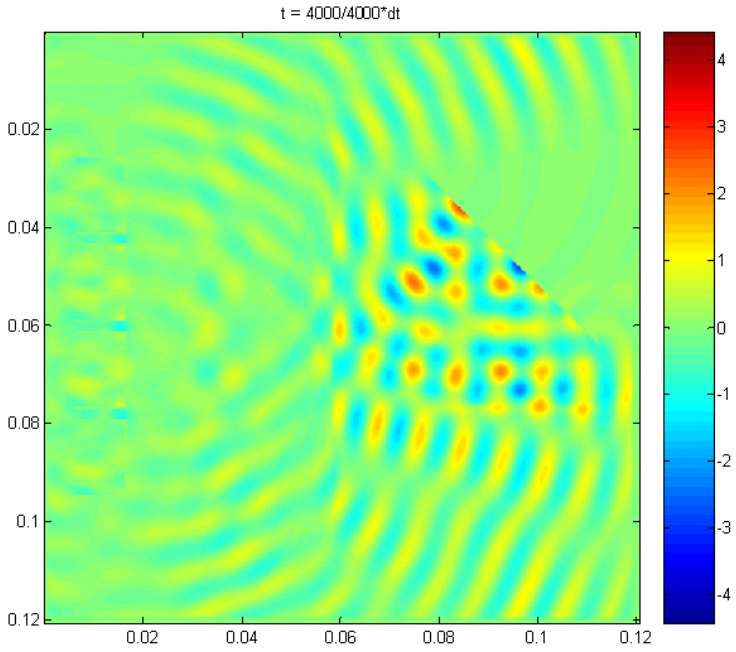

Figure 3.3: Simulation result for the input at Figure 3.2

Beyond reflectivity simulations, the phased array system is also simulated during the design stage. By assigning different signals to each transducer element, the phase delay between the elements can be achieved in simulation. Figure 3.4 shows a phased array simulation, where the transmitter array is placed in the specified rectangle. By applying required phase delays between the signals of each element, a 5° focusing

angle is achieved.

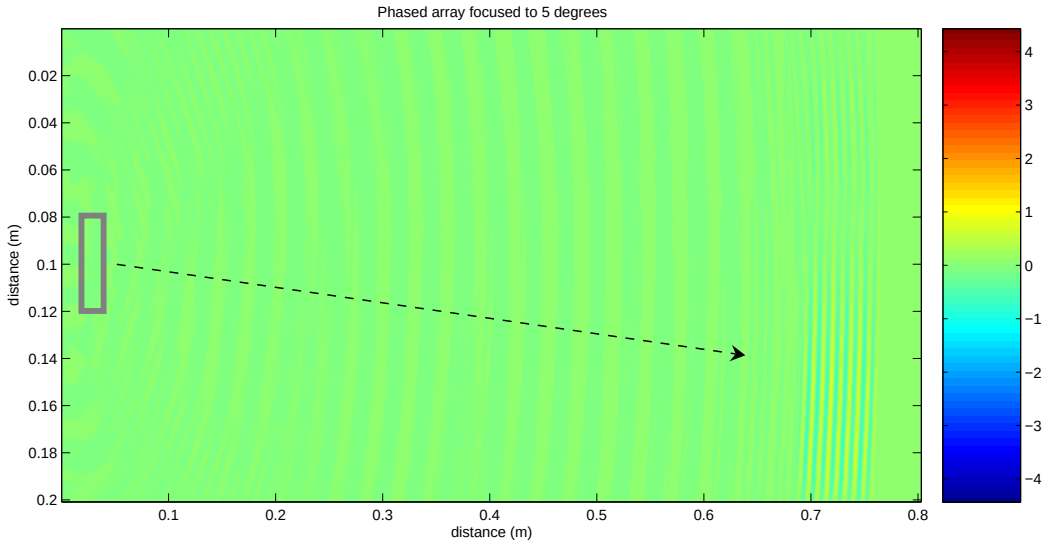

Figure 3.4: Phased array simulation (array is focused to 5°)

The phase differences between the elements can be set very accurately for a phased array simulation. This feature allows a feasible simulation of the acoustic phased arrays. Similarly the received echo from the object is saved with its full wave shape, where the phase information can be derived. By means of the phase information, this code can be used for edge-detection, identification of reflector geometry [37], determining the effects of specular scattering and diffraction [3], sonic crystals and waveguides [35], and other purposes. The main reason for implementing the FDTD method in a Matlab code is to develop a simulation environment for acoustic phenomena.

Chapter 4

Design of the Acoustic Phased Array System/Device

Most of the developed ETA devices, based on acoustic, optic or both, rely on a single transmitter element. By using a single beam only the distance of the object can be measured. In order to locate the obstacle correctly the user has to perform the scanning operation manually by rotating the device. In a similar manner the devices, which use mechanical scanning, have to be pointed in the relevant direction for detecting the objects (more explicitly stated in Section 1.2). However, by using echolocation, an array of ultrasonic transducers can locate obstacles in front of the user and provide both their angular position and distance [26].

In many applications the phased arrays are used, since it is necessary to have high gain and a directive characteristic in both electromagnetics and acoustics. Enlarging the dimensions of a single element concludes to higher gains; however directivity of an antenna or an acoustic transducer can be increased by using multielements. This new structure, formed by radiating elements, is referred as an *array*.

For an imaging application, the radiation pattern of the array is very important in order to focus the beam to a predetermined direction. To get a directive pattern, the fields coming from a single element of the array should interfere constructively in the desired direction and interfere destructively at the other directions. The interference pattern of the fields radiated from the elements, which also called as directivity pattern, can be controlled by changing the geometrical configuration of the elements, the relative distance between the elements, the phase difference between the elements and the radiated power from the individual elements [29]. Beyond these criteria, the radiation pattern of the single element also has a significant effect on the overall pattern of the array.

4.1 Transducer Selection

Before constructing the ultrasonic transducer array, a proper transducer element must be selected. The active area of the acoustic transducer is an important criterion, while selecting the transducer. The transducers which have smaller active areas will behave as point sources and transducers with active areas bigger than wavelength will behave as planar wave sources. For constructing a phased array the beam width of the individual elements are crucial; they determine the overall radiation pattern and limit the beam width of the array [29].

Other than the beam width, the working frequency of the transducer has to be selected carefully. Minimum working frequency of the transducers must be 20 kHz, which is the lower limit of ultrasound. For an upper limit it is chosen as 100 kHz, since pulsing and receiving processes will be done by a microprocessor. The final device will perform a sector scan, which needs to change the phase delay between the elements in order to change the angular sampling spacing. Implementing the phase delays for a 1 MHz ultrasonic transducer will be impossible while working with an ordinary microprocessor. 10 degree phase delay between two elements at 1 MHz corresponds to 28 ns. The calculation overhead of the new phase delay is estimated as 6 clock cycles for an ordinary microprocessor (the array has 4 elements and phase delay should be changed three times for each elements after the first one). After a simple calculation, shown in Table 4.1, digitally controlling such phase delays are difficult and also need a fast processor. For this reason, a suitable transducer for this application has work in a frequency range between 20 kHz and 100 kHz.

Transducer Frequency	10 degree Phase Delay	Calculation Overhead	Minimum Required CPU Frequency
50 kHz	560 ns	6 cycles	10.7 MHz
100 kHz	280 ns	6 cycles	21.4 MHz
1 MHz	280 ns	6 cycles	214 MHz

Table 4.1: Transducer frequency and required speed for microcontroller

Firstly, a *Polaroid transducer* (Senscomp 7000 series transducer) is selected for the imaging application. The objects up to 10 meters can be detected by using the Polaroid transducer, which works at 49.4 kHz. It has a half power beam width of 30 degrees, which is very limiting but still it can be used for constructing an array. However it has a very big disadvantage for the acoustic imaging application since it is an electrostatic transducer. An electrostatic transducer needs high voltages during the excitation for vibrating a stretched thin diaphragm. Amplitude of 400 volts peak-to-peak is needed to excite the transducer during the transmission, which means that power consumption is very high. During the transmission period, Polaroid transducer consumes nearly 10 Watt for excitation. Since one of the possible applications of ultrasonic phased array device is mobility aid for visually impaired people, low power consumption is an important issue [38].

Reducing the range of the acoustic transducer array will significantly decrease the power consumption, so a new detection range is determined. After several test and measurements with Polaroid transducer, it is observed that detecting objects at 10 meters is not necessary. Both in robotic applications and mobility aid for visually impaired people it is not required to detect more than 3 meters. Walking speed of a visually impaired pedestrian in an unknown place is 1.5 km/hour, the time taken to travel 1 meter is 2.4 seconds [39]. Considering the movement speeds of robots and visually impaired people, the new sampling region is determined. After reducing the object detection range to 3 meters, it is decided to use a piezoelectric transducer for lower power consumption.

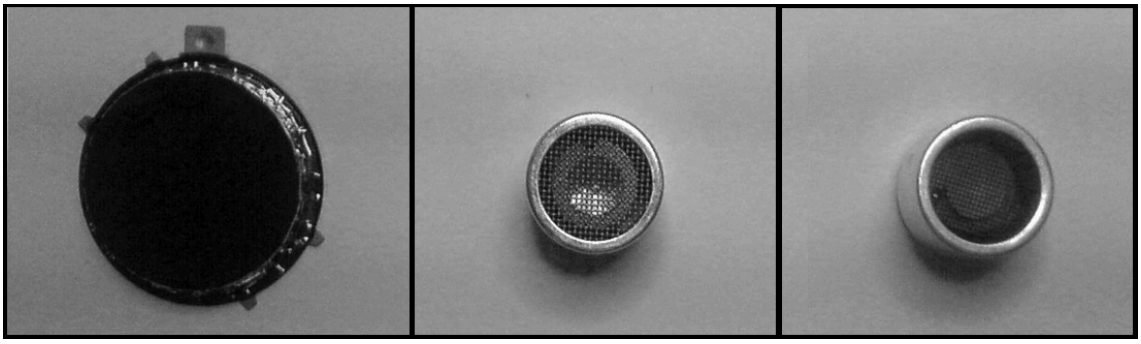

Figure 4.1: Polaroid transducer, SRF04 Transducer, Off-the-shelf Transducer with unknown specifications(respectively)

Different kinds of ultrasonic transducers are examined for their suitability to this application. Some commercial off-the-shelf transducers with unknown specifications and a Devantech SRF04 Ultrasonic Range Finder, which has its own pulsing and receiving circuitry, are tested for their compatibility as an individual element of phased array. Their power consumptions, radiation patterns, and ranges are measured (Table 4.2), and then these data are evaluated as selection criteria for finding the most suitable transducer for the ultrasonic phased array device.

	Polaroid Transducer	SRF04 Transducer	Off-The-Shelf Transducer
Type	Electrostatic	Piezoelectric	Piezoelectric
Power Consumption	10 W	0.79 W	0.7 W
Frequency	49.4 kHz	40.8 kHz	39.8 - 40.9 kHz
Detection Range	10 m	3 m	2.25 m
HP Beam Width	30 degree	43 degree	36 degree

Table 4.2: Transducer features

It can be seen form Table 4.2 that for reasonable power consumption the SRF04 has the best specifications; 3 meter detection range and a half power beam width of 43 degree. Therefore it is decided to use the transducers of the SRF04 Ultrasonic Range Finder as a phased array element. The transducers of SRF04 is unmounted from its original board, since its pulsing and receiving circuitry do not allow creating a phased array structure. After transducer selection process is finished, the design period of the ultrasonic phased array has started.

4.2 Ultrasonic Phased Array Design and Design Parameters

In the design of an array, the most significant parameters are the number of elements, spacing between the elements and their configuration, half power beam width, directivity, excitation phase and amplitude, and side lobe level. Before the design process, some of these parameters must be specified according to the application then the others are determined.

The geometrical configuration of the array and the relative distance between the elements have to be set initially, as the first step of the design process of ultrasonic phased array. There are lots of array configurations; linear, circular, spherical, rectangular, etc. [29], but the most suitable one for this application is the linear configuration, since acoustic imaging for robotic applications and mobility aid for visually impaired people does not need a three dimensional sketch of the environment in other words it is not necessary to have a two dimensional array configuration. After choosing the geometrical configuration of the array, the next step is specifying the placement strategy.

During the realization of the ultrasonic phased array device one of the most arduous problem is the placement of the transducers. The most difficult criterion to satisfy is usually the requirement of half wavelength spacing between elements in order to avoid the occurrence of unwanted grating lobes in the array response. Because of constructing the array with general purpose transducers, this criterion can not be satisfied. Thus, the placement of transducers is determined with a goal of constructing a compact device. For this reason the transmitter array is formed by aligning the transducers with minimum spacing between them which was 2.11λ.

Beyond the geometrical configuration of the array and the placement of the elements, there is another important parameter for constructing the phased array; the number of the elements. Before choosing the number of transducers to be used in the phased array, the required resolution has to be determined. More elements and closer placement correspond to higher resolution, adversely less transducers and more distances between them end up to a less complicated device with a low resolution. For an optimum resolution the focusing angles has to be selected according to the application, since the resolution of the system is determined by the angular sample spacing. The minimum angular difference between the focusing angles of the array is calculated as 2.5 degrees. For the applications of robotics and mobility aid for visually impaired people, the angular sample spacing of 2.5° is adequate, where 2.5° means that 109 mm spatial resolution at 2.5 meter and 13 mm spatial resolution at 0.3 m.

With respect to aforementioned criteria and specified angular sampling spacing, directivity patterns of the different array structures are simulated and the number

of elements is chosen. Array factor as stated in Equation 2.13 for different arrays constructed from three, four, five, and six transducers are calculated with Matlab. Increasing the number of elements gives better directivity patterns, but there are other parameters like power consumption, complexity of the system and compactness of the device. Therefore, the number of the elements in the phased array device has to be as small as possible; so the array is constructed with four transducers.

After setting the most of the parameters for array design, the receiver array has to constructed. The system's overall performance is directly related to both transmitter array and receiver array, so the construction of receiver array has to be performed carefully.

4.2.1 Placement Strategy

After constructing the transmitter array and calculating the phase delays according to Equation 2.16, the radiation pattern of the array is measured. The gain measurements show that 2.11λ spacing between transducers and larger phase delays (comparable with $\pi/2$) are causing large grating lobes inside the active area. In Figure 4.2 the transmitter array is focused to -5° and it can be easily seen from the figure that there is a big grating lobe at 23°. The amplitude of grating lobe is smaller than the main beam, because of the directivity pattern of a single transducer; element factor.

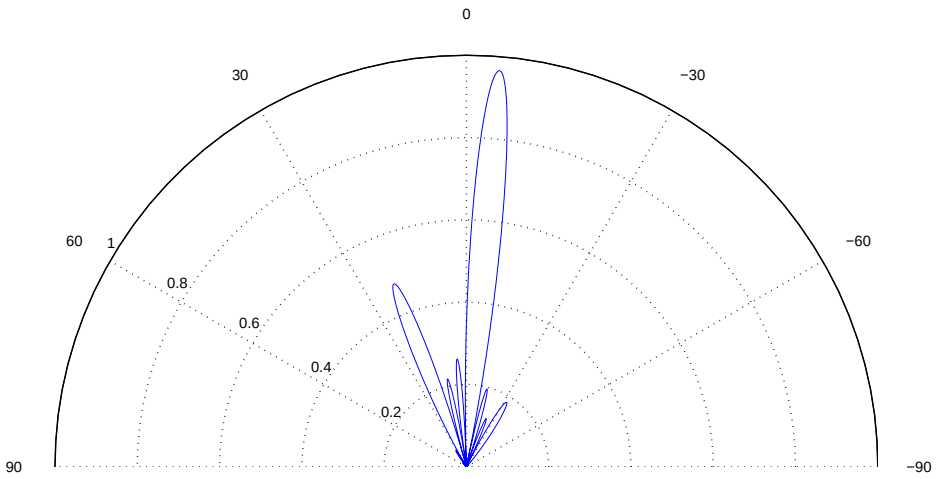

Figure 4.2: Radiation pattern of Transmitter array

This grating lobe decreases the field of view (FOV), which is the steerable active area covered by the main beam where no grating lobes appear. Actually, this grating lobe is one of the other maximum points in the array response. The maxima[1] of the array is calculated by the equation below, recall the Equation 2.15:

$$\theta_m \;=\; \cos^{-1}\left[\frac{1}{kd}\left(-\beta \pm 2\mathrm{m}\pi\right)\right]$$

For 2.11λ spacing between the elements the FOV is 28.3° (Equation 4.1). But in this application, the placement can not be smaller than 2.11λ for transmitter array (less than one wavelength spacing is needed for a FOV of 90°).

$$\sin(\mathrm{FOV}) \;=\; \frac{\lambda}{d} \quad (\text{applies for } d > 2\lambda) \tag{4.1}$$

In order to eliminate these grating lobes, the placement of receiver array is done with a different strategy. If the transmitter array has the spacing of d, by setting the spacing between the element of receiver array to $1.5d$, $2.5d$, $3.5d$, etc. the receivers response become different than the transmitter array's. This approach makes the receiver array to have the second maxima at one of the nulls of transmitter array and also makes the transmitter array to have the second maxima at one of the nulls of receiver array.

By using the spacing of 2.11λ, the FOV of the overall system can not be larger than 28.3° with identical receiver and transmitter arrays. But in this case, the grating lobe of the system appears at the third maxima rather than the second one, which is canceled by a null in the receiver arrays response. By using off-aligned receiver and transmitter arrays, the grating lobes moved away for the overall system. With 2.11λ spacing the FOV is 28.3°, but by applying this placement scheme the FOV for the overall system is doubled.

For this reason, the receiver array is formed with 5.14λ spacing between each transducer (it should be 5.27λ for an exact cancellation). By forming the receiver array and the transmitter array non-identical, the directivity pattern for transmitter array and receiver array becomes different. The red one shows the directivity pattern of the transmitter array and blue one shows the directivity patter of receiver array in Figure 4.3, in which both arrays are focused to -5°.

[1] *Maxima* is the point where the function has its maximum value.

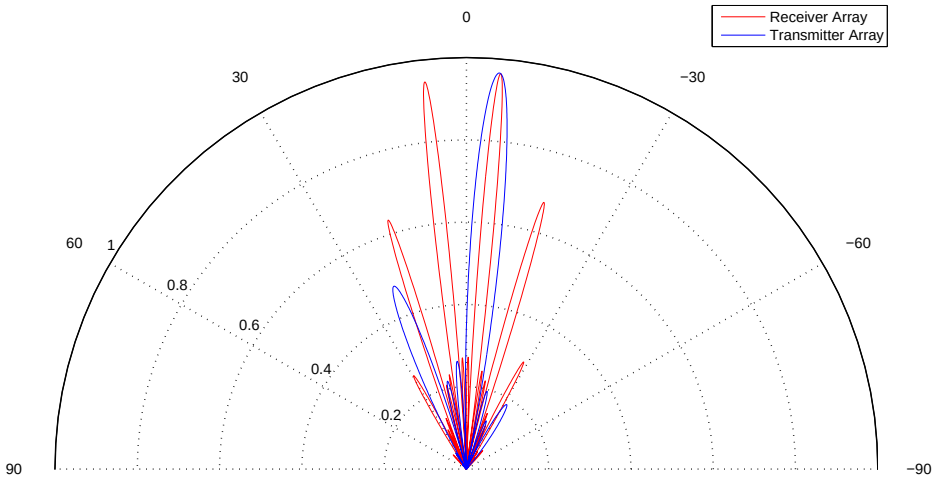

Figure 4.3: Gain of Receiver array

The of-alignment between receiver and transmitter arrays causes the grating lobes to appear at different places. Since the overall gain of the system is the product of receiver gain and transmitter gain, the grating lobes diminish for the overall system (Figure 4.4). This is also referred to as *pattern multiplication* for arrays of identical elements [29].

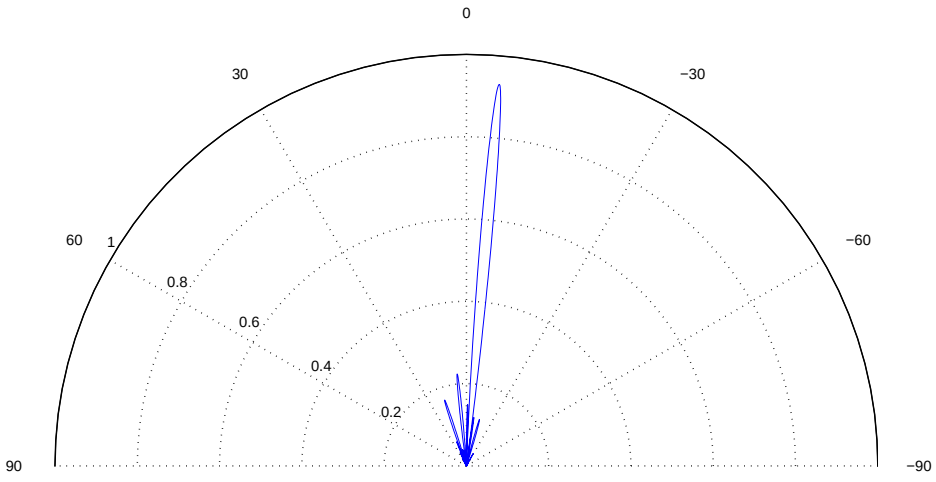

Figure 4.4: Gain of overall system (TX × RX)

If the Figure 4.4 is observed carefully, it can be easily seen that the intensity of the overall system is not normalized. The array factor is normalized to one, but

the calculations also include the directivity pattern of transducers, element factor. Since the gain of SRF04 transducers are taken into account, the intensity of the overall system decreases with the increasing sampling angle.

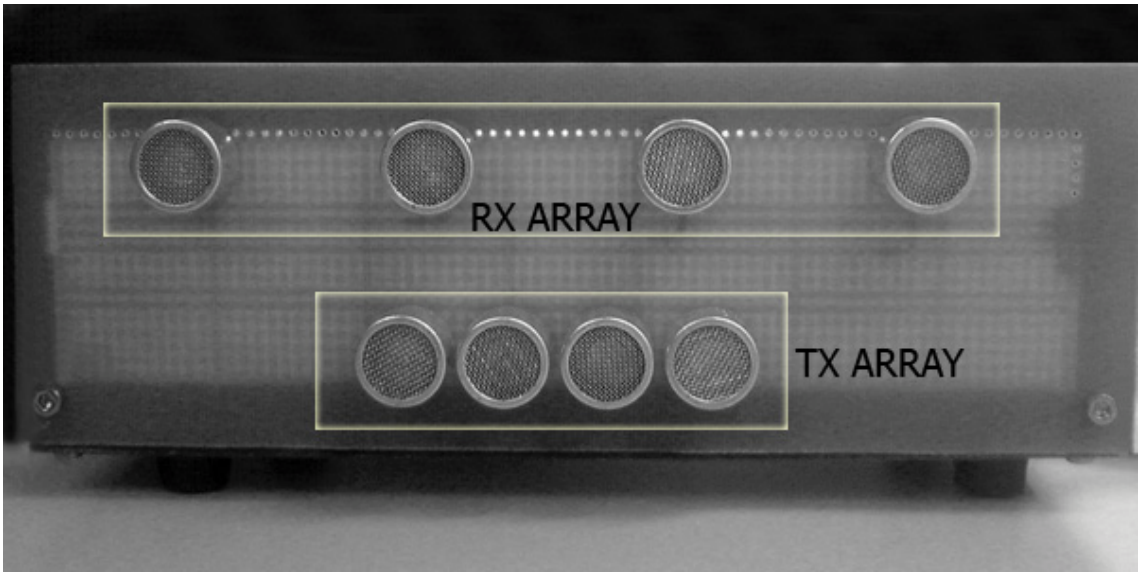

Figure 4.5: Receiver and transmitter array

After analyzing the directivity patterns above, the arrays are constructed with the aforementioned placement strategy. Two linear arrays are realized with using the SRF04 transducers, one for transmitting acoustic pulses and the other for receiving the returning echoes. Figure 4.5 shows the constructed array, which will be used for echolocation.

4.3 Design of Driver and Readout Circuits

The circuitry of the ultrasonic phased array device is basically divided into there modules; transmitter, receiver and controller. The transmitter module sends out ultrasonic bursts of acoustic energy through the ultrasonic transducers. The receiver module detects the echo coming from the obstacles in the beam path. A microcontroller controls both transmitter and the receiver modules.

While transmission, microcontroller sets the phase delays between each elements of the transmitter array. The detected echo coming from the receiver array is sampled with an internal ADC by the microcontroller. By using the phased array

principle the r and θ between the object and device can be determined, shown in Figure 4.6.

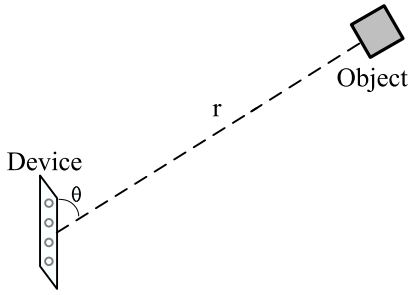

Figure 4.6: Object placed with an angle of θ and distance of r

The location of an object can be calculated by using the speed of the sound in air. The resolution of r and θ depend on the ADC sampling rate, and array structure.

4.3.1 Pulse Generation and Driver Circuitry

Before deciding to use a microcontroller, the pulse generation was done by using a 555 timer chip. Timer chip produces continuous pulses at the working frequency of transducers. The transmitters can not be fed directly with the generated pulse form the timer chip, because transmitters have to wait for the receivers to detect the echo. For detecting a 3 meter range the time delay between two transmissions there should be least 17.5 msec, which is the required time of flight for 6 meters (both the transmitted sound wave and the reflected echo need to propagate 3 meters).

In order to provide the required time delay between two transmissions, three counters are used as a frequency divider. By using the different output ports of counters a pulse with 0.4% duty cycle is generated. Then, by logically ANDing the outputs of the counters and timer an eight cycles of 40.8 kHz pulse is achieved at a frequency of 40.8 Hz (Figure 4.7). An eight cycle burst pulse is transmitted rather than using a single cycle pulse, because it is more efficient when detecting adjacent objects. Some animals, like dolphins, also use burst pulses for echolocation [40].

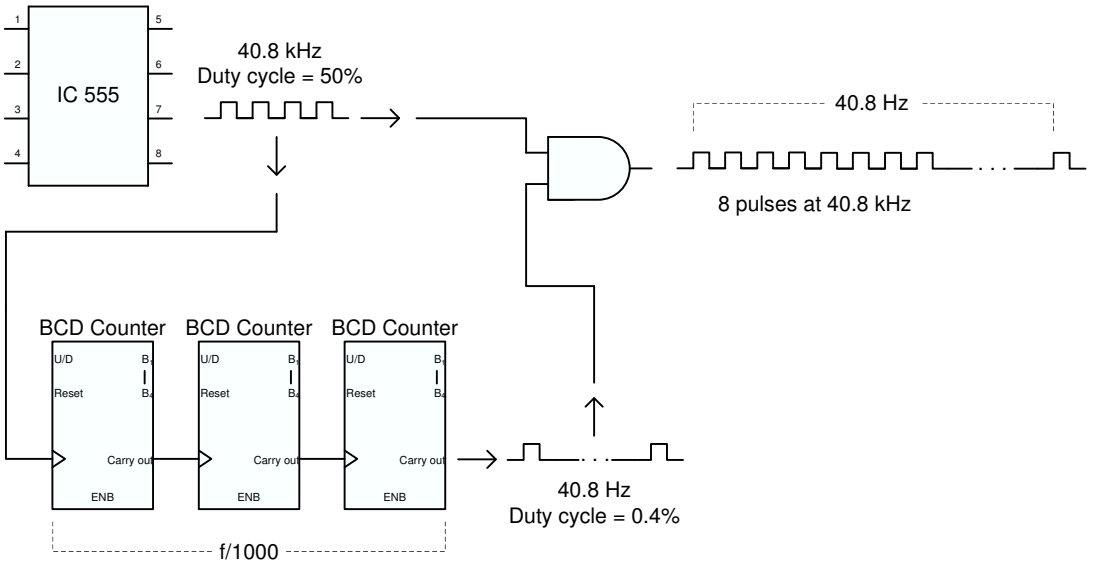

Figure 4.7: Pulse generation

Since the pulse generation circuit can not drive transducers alone, two different driver circuits are designed Figure 4.8 and Figure 4.9. Both circuits get the generated pulsing signal, described above, as an input and transfers it to the transducers by increasing its driving strength.

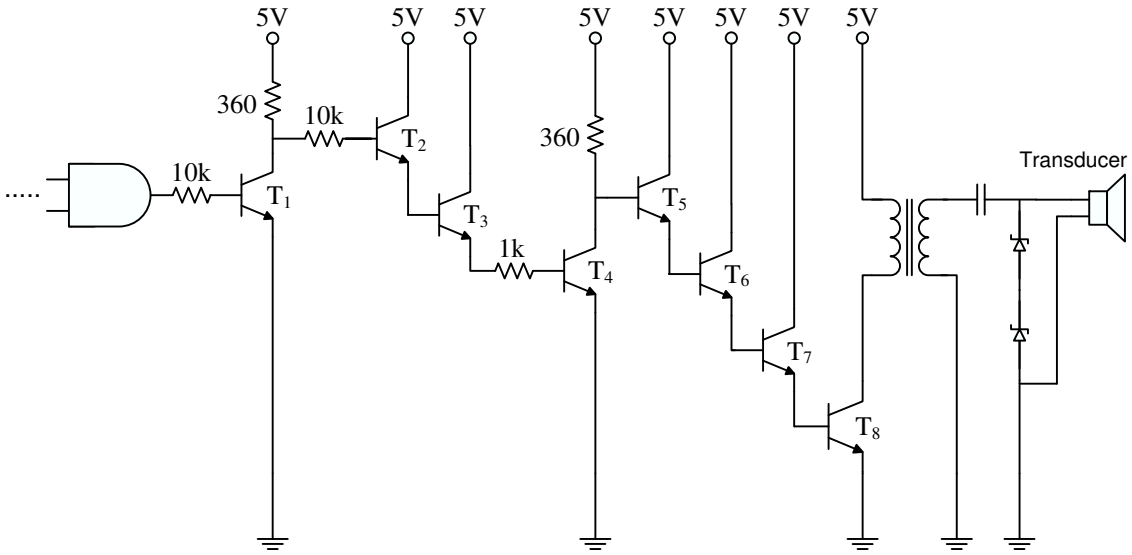

Figure 4.8: Powerful Driver circuitry

In Figure 4.8 all transistors are general purpose npn transistors except T_8, which is a power transistor and can handle a continuous collector current of 2A. These

transistors are used for improving poor driving capability of AND gate, which is in order of several milliamperes and the voltage at the output of the logic gate suddenly drops if higher currents needed. For this reason, the transistor T_1 is placed at output of the AND gate. After that step there is a Darlington bridge, formed by T_2 and T_3, for current amplification. The disadvantage of the Darlington is the voltage drop due to base-emitter voltage of transistors, so T_4 is used for voltage amplification. T_5, T_6 and T_7 are used to drive the power transistor at the end. By using a transformer, high voltages can be achieved at the transducer side. The zener diodes determine the voltage level on the transducer, for example, by using two 200V zener diodes 400 volt is generated for driving the Polaroid transducers.

After deciding to decrease the power consumption and changing the type of the transducer into SRF04 transducer, there is no need to the circuitry in Figure 4.8 with such a high driving strength, aforementioned in Section 4.1. Therefore, the driver circuitry is changed with a more compact and with a less power consuming circuitry in Figure 4.9.

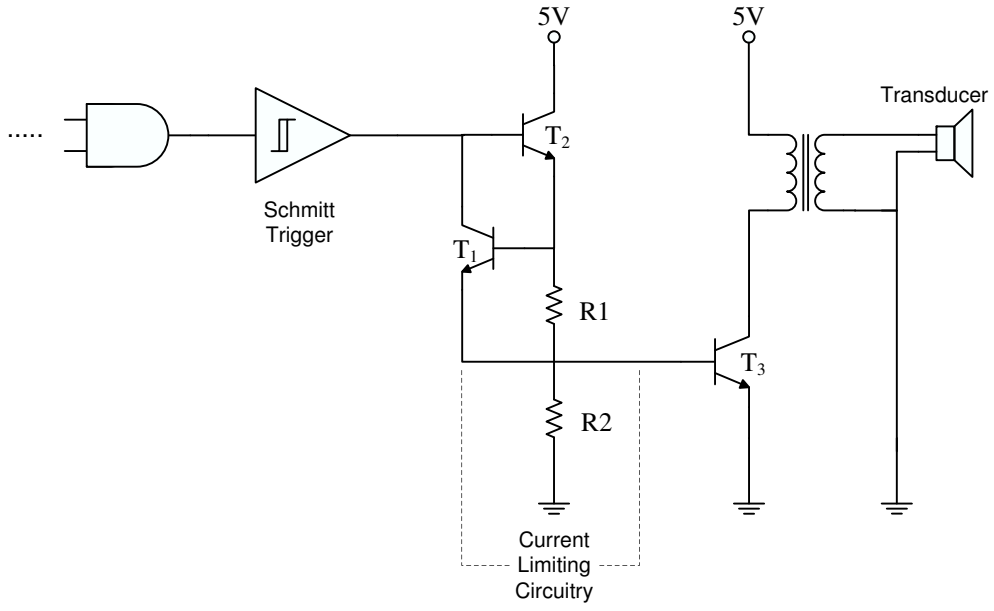

Figure 4.9: Driver circuitry

A Schmitt-Trigger is placed as a first step in order to increase current driving capability and increasing the slew rate. In the current limiting circuitry, by setting the values of R_1 and R_2 the current flow through the base of the T_3 can be controlled. The switching transistor T_3 in the last part of the circuit is a 2N2222 npn transistor,

which can handle currents up to 200mA. By using a transformer at the end, the voltage level is shifted up and a piezoelectric transducer can be pulsed. Since the power requirement is lower than a Polaroid transducer, as specified in Table 4.2.

4.3.2 Pulsing and Receiving with Microcontroller

For the scanning process it is necessary to change the overall directivity pattern of the transmitter array, where different phase delays are needed for different focusing angles. Instead of designing a different phase delay circuitry for each transducer, it is easy and more efficient to use a controller for setting the desired phase delays between the elements. If a microcontroller will be used in the system, it will be unnecessary to produce the pulsing signal with using a timer and counter chips, Figure 4.7. All of the pulsing activity and delay settings can be done by using the same microcontroller.

It is chosen ADuc7024, produced by Analog Devices, as a microcontroller, which has an ARM7TDMI core and works at 41.78 MHz. Beyond its ARM core and working frequency, the main reason for choosing this controller is its ADC. The readout process needs a fast ADC for better resolution, where the internal 12-bit ADC of the ADuC can sample with a speed of 1 MSPS. Also the power consumption of this microcontroller is not very high; it works with a 3.3 Volt supply and consumes 40 mA in active mode.

Finally, with using ADuc7024 the pulse generation is done in software and the driver circuitry is also modified as in Figure 4.10.

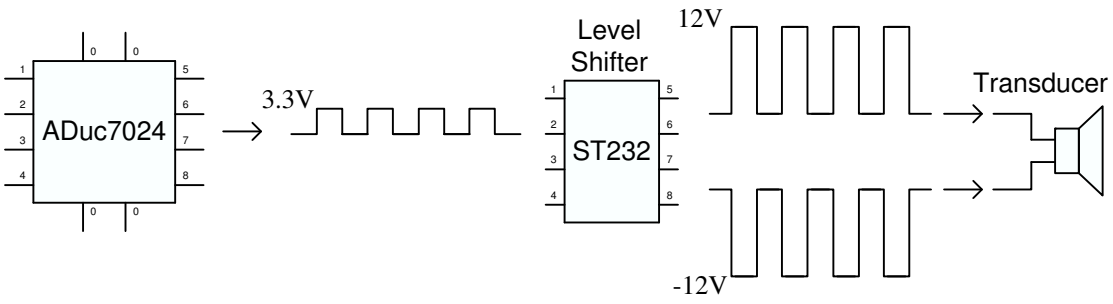

Figure 4.10: Pulse generation and driver circuitry with microcontroller

ST232 is a simple RS232 level shifter with an output driving strength of 60mA. Rather than using the pre-designed circuits in Figure 4.8 and Figure 4.9, it is better to work with a single IC. Usually, level shifters are not produced with high output driving strengths but in this case ST232 is an exception. By using it a piezo transducer can be driven in a bipolar form, where with a single input signal the two different outputs can be generated as in Figure 4.10 and transducers can be pulsed successfully.

The received echo from the receiver array is not connected directly to the ADC input of microcontroller; a filtering unit is added before sampling the incoming data. A simple bandpass filter is designed to suppress the 50Hz noise and harmonics of the transducer at higher frequencies. With using two CMOS OPAMPS a lowpass and a highpass filter is formed, where the active filters have an overall gain of 10 (Figure 4.11). The sampling rate of the analog-to-digital conversion is internally adjusted with software. This flexibility over ADC allows to sample in higher rates for better resolution and in lower rates for a real-time application.

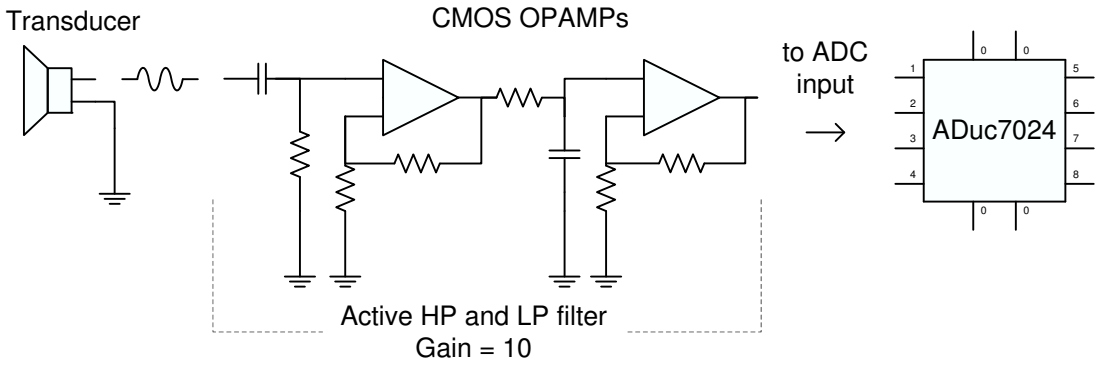

Figure 4.11: Receiver circuitry with microcontroller

Chapter 5

Experiments

This chapter will describe how measurements and the experiments are done for the system described in the previous chapter.

5.1 Gain Measurements

The gain measurement setup is constructed as in Figure 5.1 and directivity patterns of both the transmitter array and the receiver array are measured with this setup. In spite of changing the place of transducer for every measurement, the device is rotated around itself, where the rotating platform has a sensitivity of 2.5°.

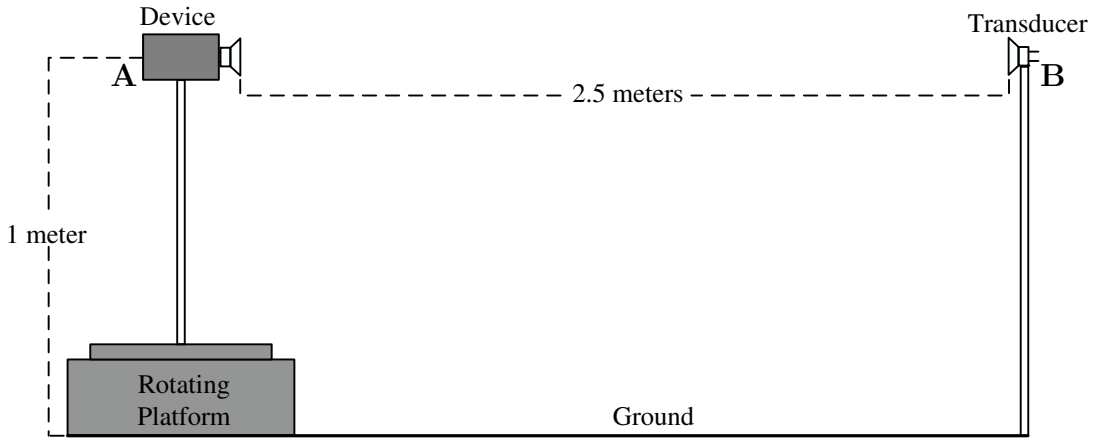

Figure 5.1: Measurement setup

In general, the gains or directivity patterns of acoustic transducers are measured

in an anechoic chamber [1]. In this work, the measurements are done in a sufficiently big room, where most of the reflections are from ground. The shown false path from the ground in Figure 5.2 can be easily identified. If the intensity of the beam traveling through the direct path between the device and the transducer is normalized to 1, the contribution of the false path over the direct beam is 0.09. Also, in a transient analysis the false path from the ground can be easily separated from the direct beam, because the path differences between them causes a delay in time.

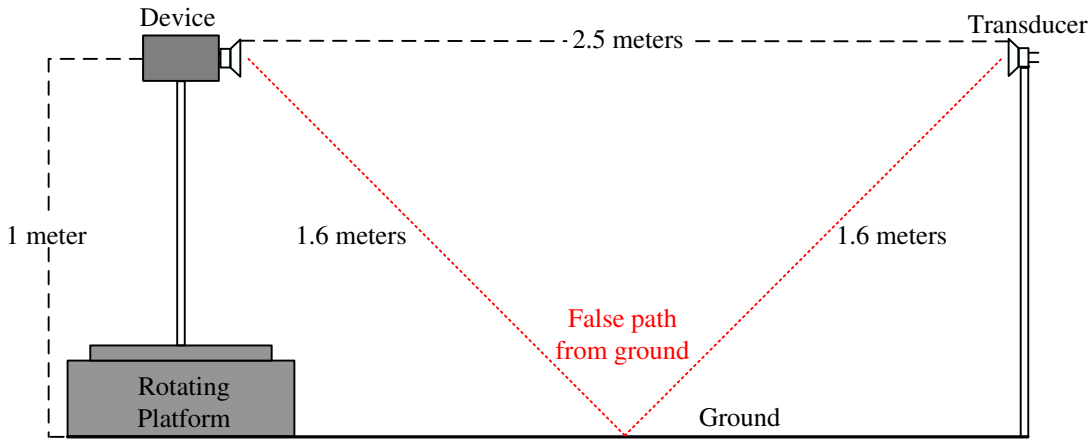

Figure 5.2: False path from ground

5.1.1 Directivity Pattern of Single Transducer

First of all, to verify the accuracy of the measurement system, the gain of a single transducer is measured relative to another transducer. Since its gain is known by [41], it is the best way to test the measurement setup. In Figure 5.3 the dashed red line shows the gain of a single SRF04 transducer, given by its datasheet. Blue line is the measured gain of single transducer. The area of the interest is restricted from -$\pi/3$ to $\pi/3$, else there are only negligible side lobes.

For measuring the directivity pattern of single transducer, a single transmitter is replaced on the rotating platform (place **A**) in Figure 5.1 and a receiver transducer is placed at **B**.

[1] *Anechoic chamber* is a room in which there are no acoustic echoes caused by reflections from the internal surfaces of the room as well as no external noise

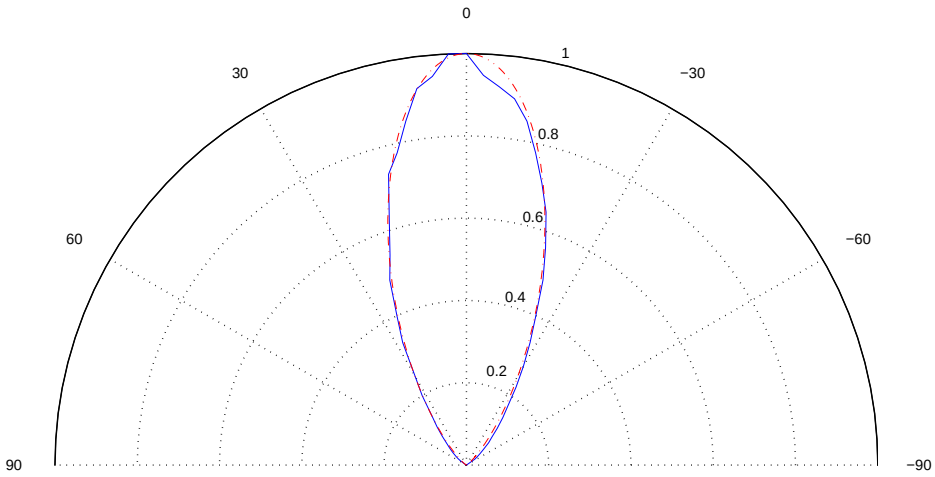

Figure 5.3: Gain of single transducer

5.1.2 Directivity Pattern of Transmitter Array

For measuring the directivity pattern of transmitter array, the device in Figure 5.1 is run in transmitter mode and the transducer is used as a receiver. The dashed red line shows the theoretical array response as stated in Section 4.2, and the blue line shows the measured directivity pattern of the transmitter array (Figure 5.4).

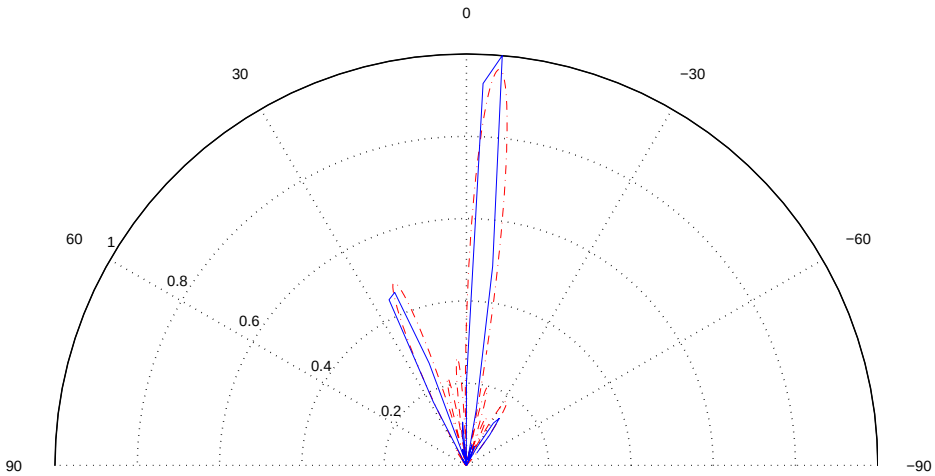

Figure 5.4: Gain of transmitter array

5.1.3 Directivity Pattern of Receiver Array

For measuring the directivity pattern of receiver array, the transducer in Figure 5.1 transmits ultrasonic pulses and the device is used as a receiver. The dashed red line shows the theoretical array response as stated in Section 4.2, and the blue line shows the measured directivity pattern of the receiver array (Figure 5.5)

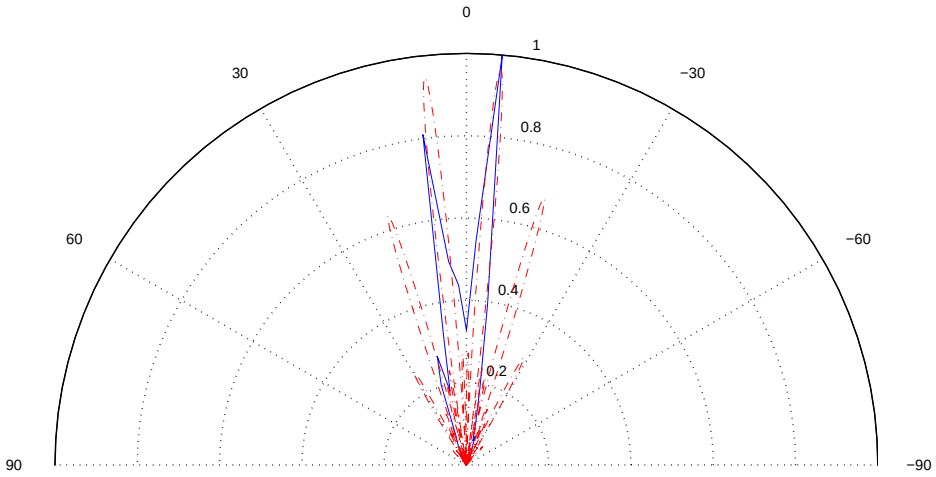

Figure 5.5: Gain of receiver array

The overall system gain is shown in Figure 5.6:

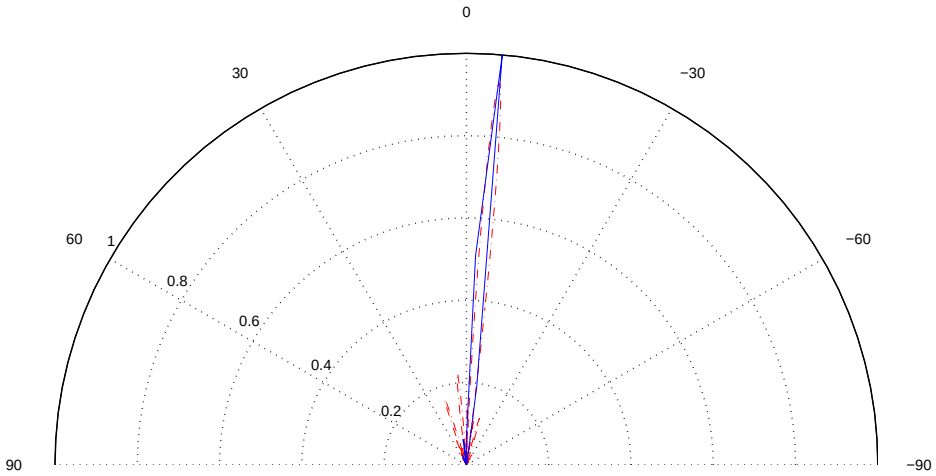

Figure 5.6: Gain of receiver array

Receiver and transmitter arrays' directivity patterns are measured for each angles. All of the directivity patterns for different angles are given in Appendix A.

5.2 Experiments

After analyzing the performance of the system, it is decided that the current system performance is adequate for acoustic imaging. Some experiments are done with randomly positioned different objects.During the experiments the device is set with the following parameters:

Parameter	Value
Scanning Range	0.2m to 3m
Field of View	30°
Distal resolution	Δr = 1mm
Angular resolution	$\Delta\theta = 2.5°$
Working frequency	f = 40.8 kHz
ADC sampling speed	600 kSps
Pulse width	8 cycles (196 μsec)

Table 5.1: Device parameters used in experiments

All of the experiments are performed with the same code running on the ARM based microcontroller. The beam steering is implemented within the range of -15° to 15° and the sampling rate of ADC is set to 600 kSps. Reducing the sampling speed of ADC reduces time of receive beam forming (less data means less processing time), but the phase information of the returning echo is important. it is unacceptable to lose the phase information of the echo in a phased array system.

The sampled echo by ADC is transfered to a computer via serial port. The receive beam forming is done with a computer by using Matlab, since the microcontroller does not have enough memory and processing speed for it. All of the experiment results are achieved after some post processing, no real-time acoustic imaging is performed.

The ultrasonic phased array device is placed at the origin (0, 0) in all of the experiments below. The detected objects seem wider, because the missing elements

in the figures are interpolated while switching from polar coordinates to cartesian coordinates.

5.2.1 Experiment I

In this experiment setup a 20 cm wide wooden block is placed 135 cm away from the device.

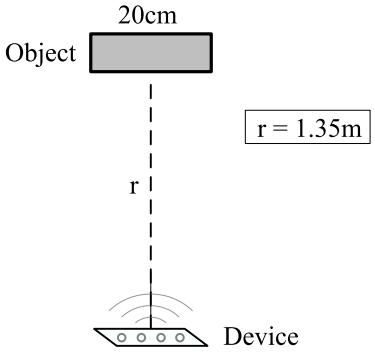

Figure 5.7: Experiment-I Setup

Figure 5.8 shows the received signal at 0° from one of the elements of the receiver array; RX-0. The transmitter array is focused to 0° and the received signal is captured by the ADC after the pulsing is finished.

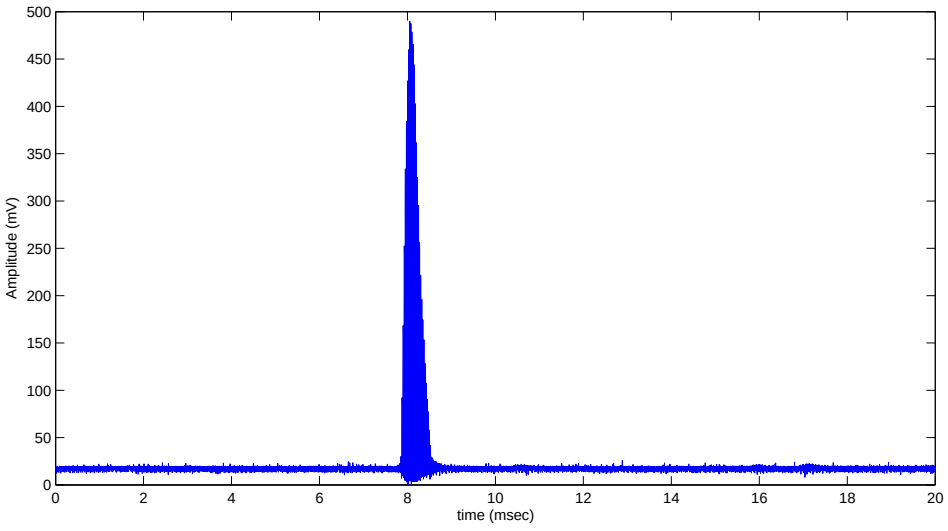

Figure 5.8: Received signal from receiver RX-0 (for $\theta = 0°$)

When Figure 5.8 is zoomed in, the returning echo from the object can be identified clearly (Figure 5.9).

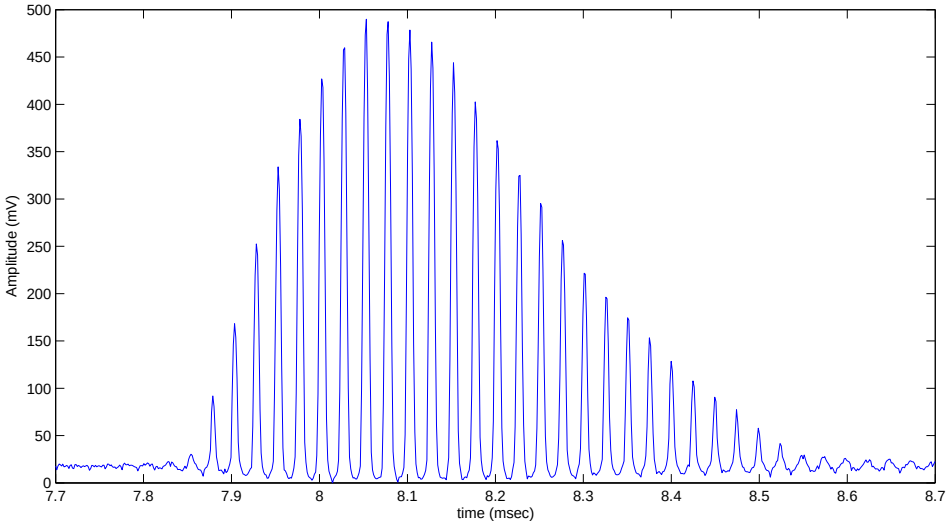

Figure 5.9: Received signal from receiver RX-0 (for $\theta = 0°$)

After the pulsing of the transmitter array has finished, not only the RX-0 but all of the elements of the receiver array receives the returning echo. The receiver array has four elements, but it is shown just three of them in order to achieve more clear figures.

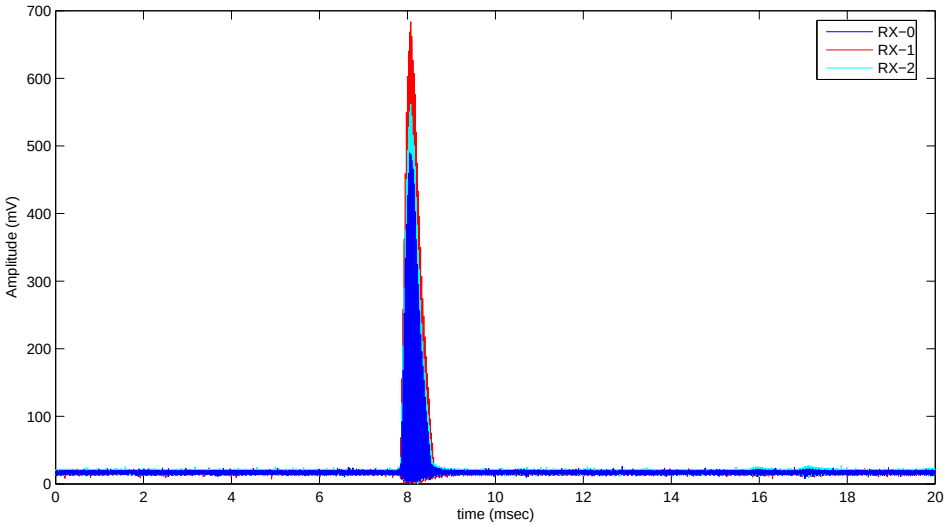

Figure 5.10: Received signal from receiver RX-0, RX-1 and RX-2 (for $\theta = 0°$)

The received signals from different elements of the receiver array are added to each other as described in Appendix B. In Figure 5.11, all of the signals are added to each other with no phase delays since the data is processed for 0°.

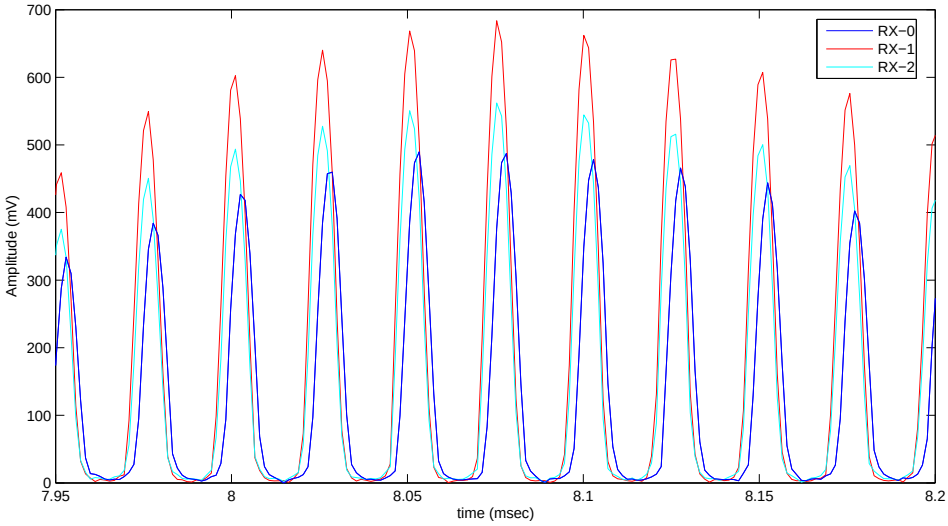

Figure 5.11: Received signal from receiver RX-0, RX-1 and RX-2 (for $\theta = 0°$)

After combining all of the signals received from the receiver array, the receive beam forming is completed for 0°. The following figure shows the processed data for 0°.

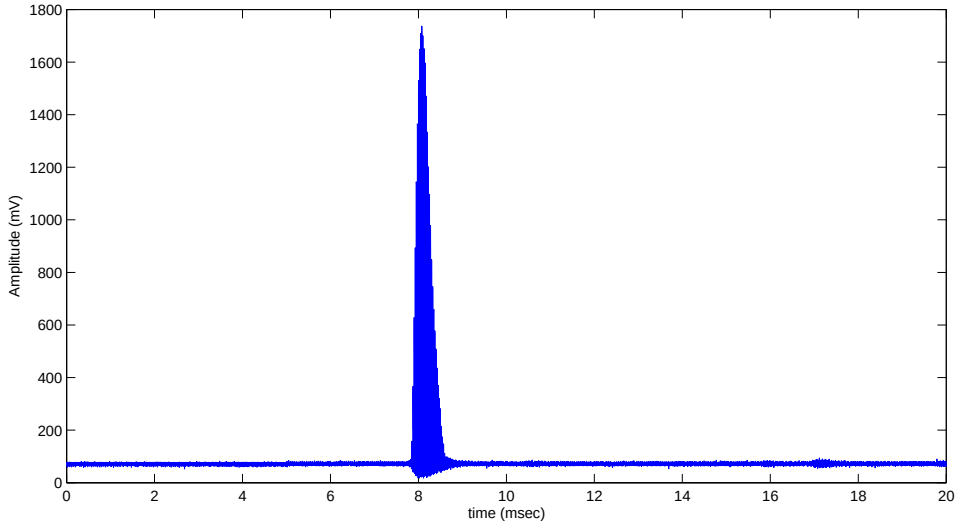

Figure 5.12: Processed signal for $\theta = 0°$ after receive beam forming

In Figure 5.13, all of the signals are added to each other with the calculated phase delays for the focusing angle of 5°.

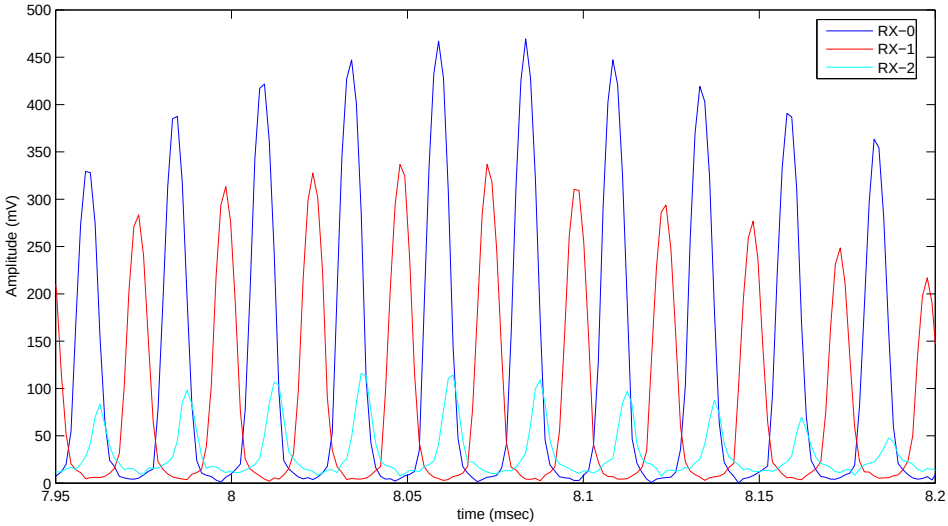

Figure 5.13: Received signal from receiver RX-0, RX-1 and RX-2 (for $\theta = 5°$)

After combining all of the signals received from the receiver array, the receive beam forming is completed for 5°. The following figure shows the processed data for 5°.

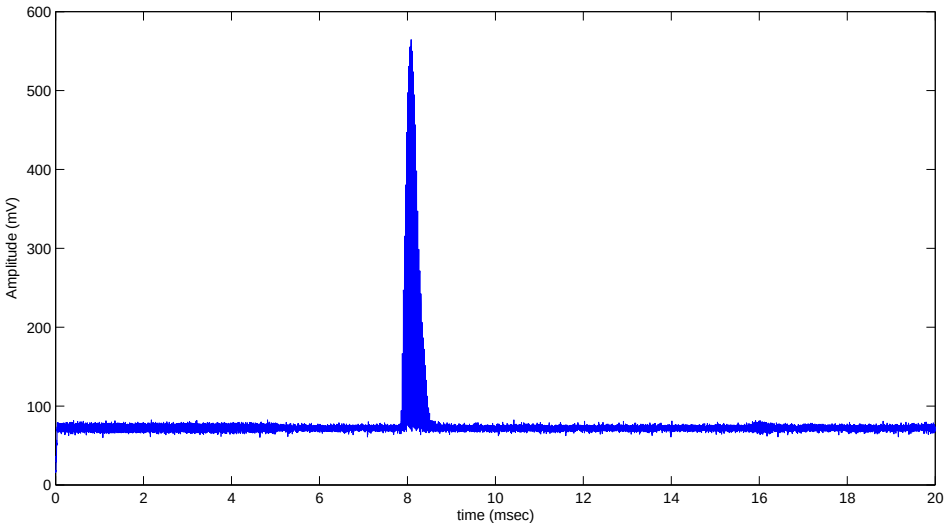

Figure 5.14: Processed signal for $\theta = 5°$ after receive beam forming

With the receive beam forming principle, the received signals are processed for each beam steering angles. After concluding with the necessary data for each angles, it is converted form polar coordinates to cartesian coordinates and the missing elements are interpolated. Figure 5.15 shows the detected object for the experimental setup shown in the Figure 5.7.

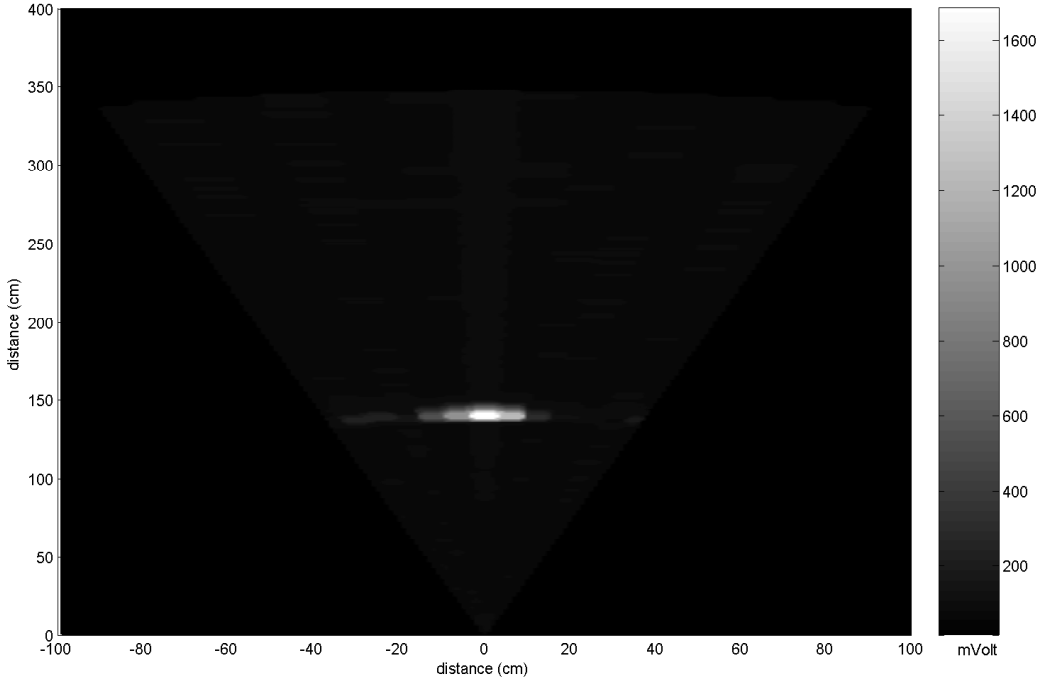

Figure 5.15: Experiment-I Result

Finally, the distance of the object can be detected easily since the wooden object is a good reflector.

5.2.2 Experiment II

A 5 cm wide wooden block is placed 100 cm away from the device with an angle of 5°. The wooden object is a good reflector, so the distance and angle of the object can be detected easily.

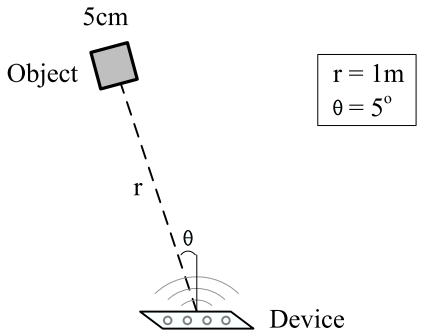

Figure 5.16: Experiment-II Setup

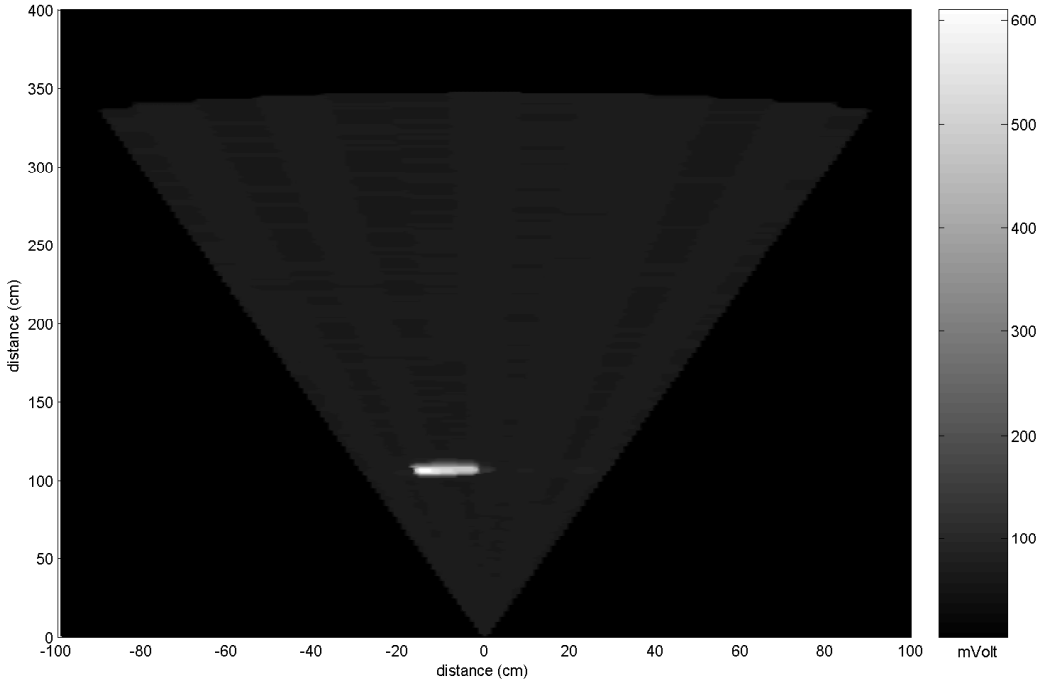

Figure 5.17: Experiment-II Result

5.2.3 Experiment III

A 20 cm wide wooden block is placed 235 cm away from the device with an angle of 4°. The wooden object is a good reflector, so it can be detected easily.

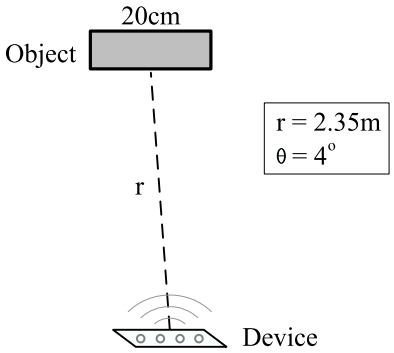

Figure 5.18: Experiment-III Setup

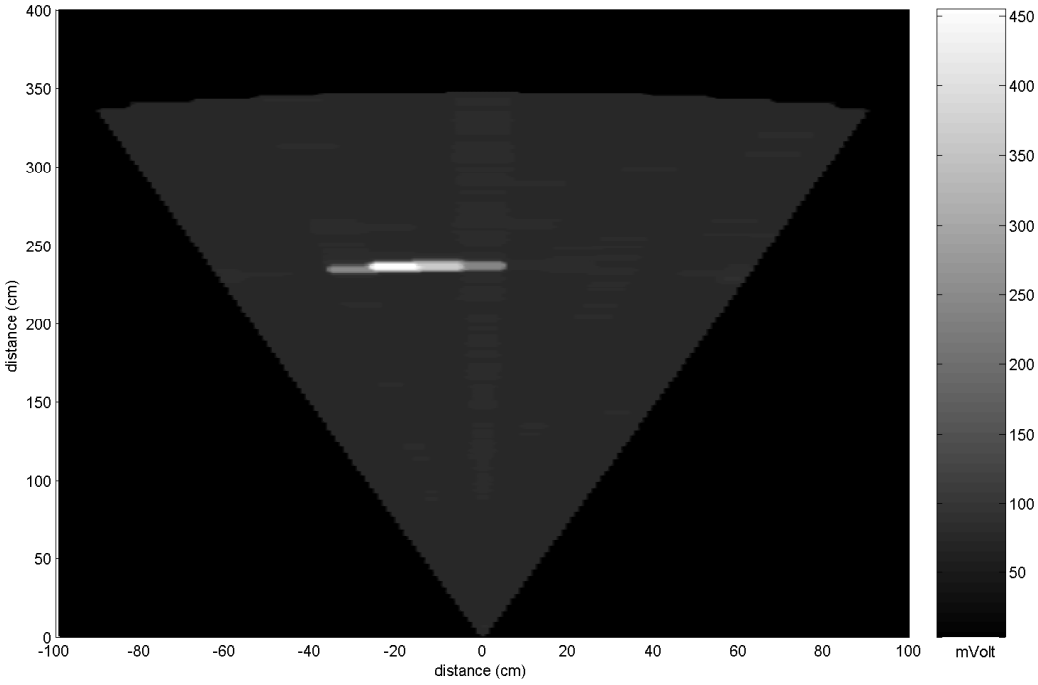

Figure 5.19: Experiment-III Result

5.2.4 Experiment IV

A 3 mm wide plastic cable is placed 65 cm away from the device with an angle of 2.5°. The over hanging plastic cable is a bad reflector, but it can be detected. Since the returning echo from this object is less than a good reflector, the background noise can be easily seen in Figure 5.21.

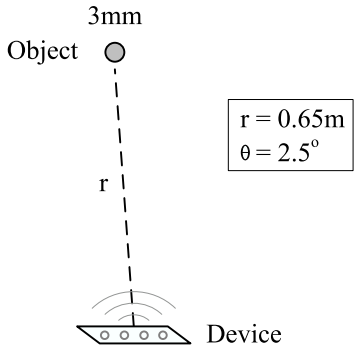

Figure 5.20: Experiment-IV Setup

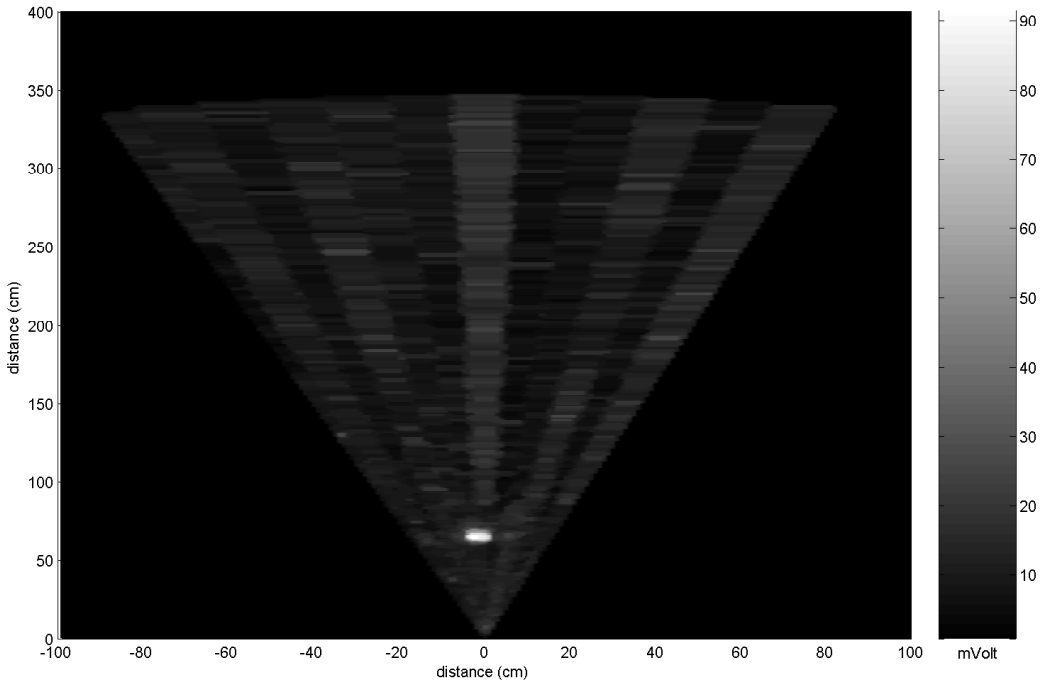

Figure 5.21: Experiment-IV Result

5.2.5 Experiment V

Two different wooden blocks are used in this experiment. A 5 cm wide objects is placed 100 cm away from the device with an angle of 7.5°. As a second object a 20 cm wide object is placed 200 cm away from the device with an angle of -5°. Both objects are detected successfully and they can be easily separated from each other as seen in Figure 5.23.

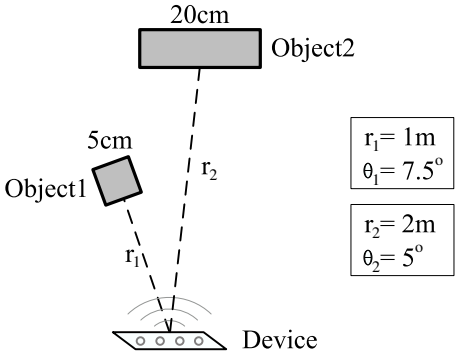

Figure 5.22: Experiment-V Setup

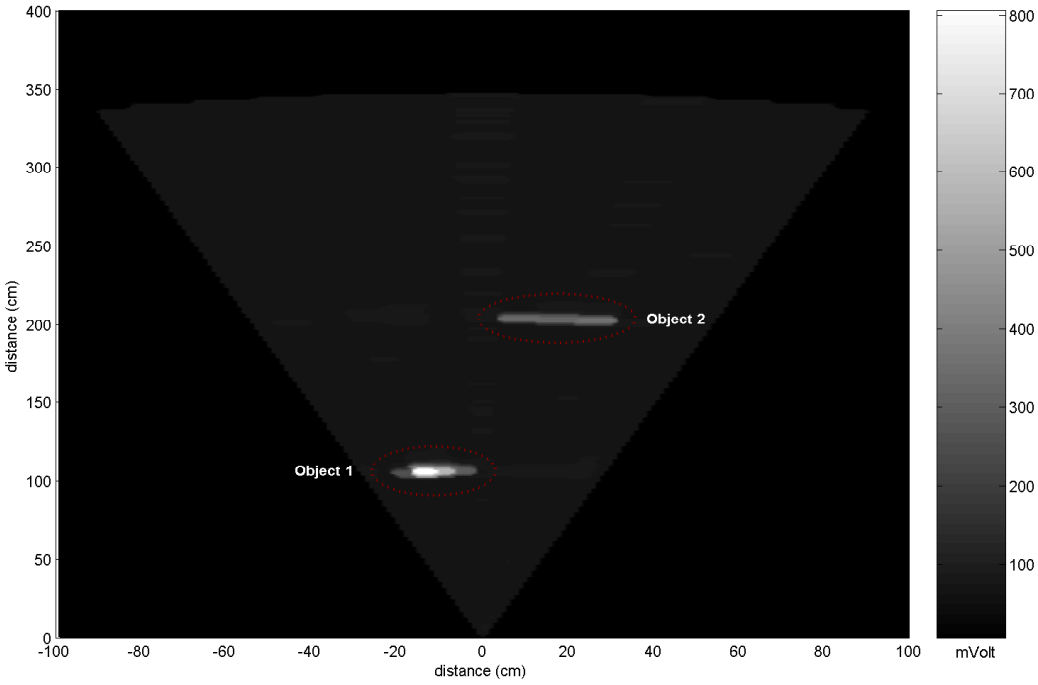

Figure 5.23: Experiment-V Result

5.2.6 Experiment VI

A 50 cm wide office chair is placed 120 cm away from the device. The office chair is coated with a soft cloth and does not have a straight surface. This object is a very bad reflector for sound, so the shape of object can not be figured completely only the presence of it can be detected.

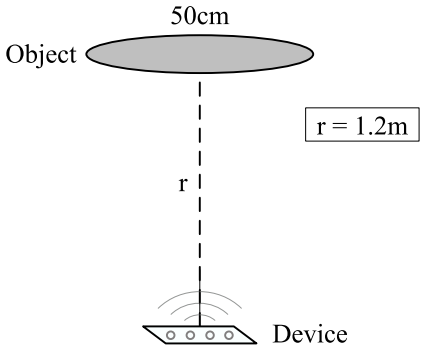

Figure 5.24: Experiment-VI Setup

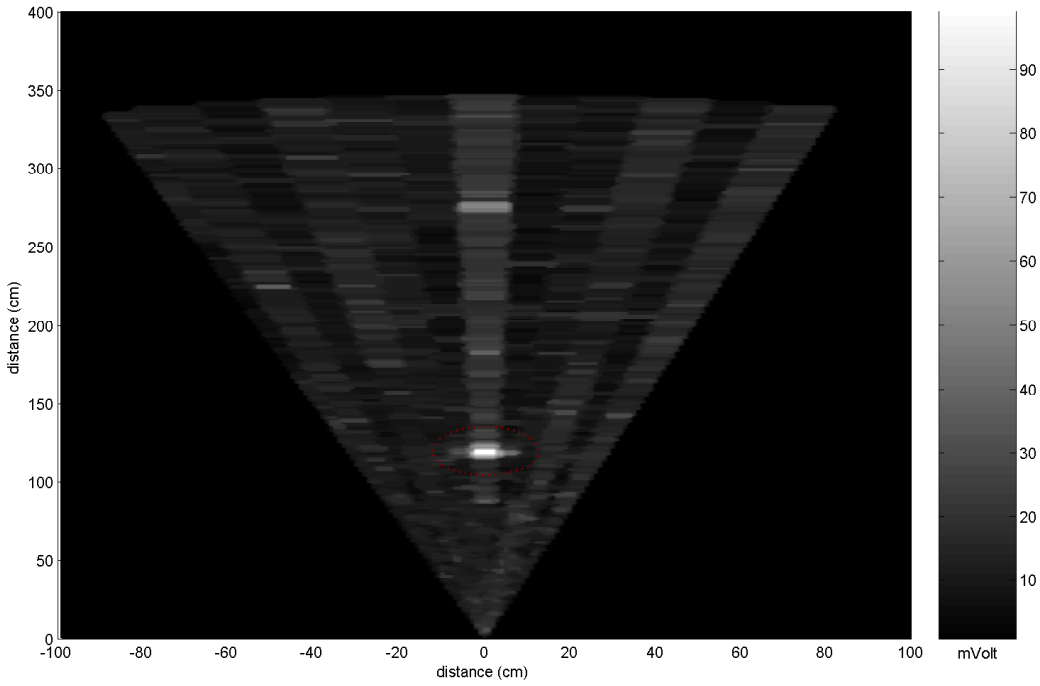

Figure 5.25: Experiment-VI Result

5.2.7 Experiment VII

A 5 cm wide metal block is placed 145 cm away from the device with an angle of 15°. The metal object is a good reflector and it can be detected easily. Although there is another problem in this case; the directivity pattern of the system at ±12.5° and ±15° have side lobes which affect the measurement. A false object is also detected in this experiment due to the side lobe at 15° while measuring the returning echo at -15° (see Appendix A for directivity patterns).

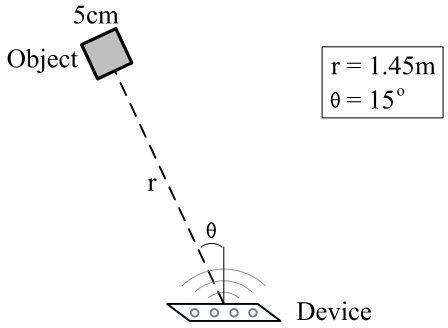

Figure 5.26: Experiment-VII Setup

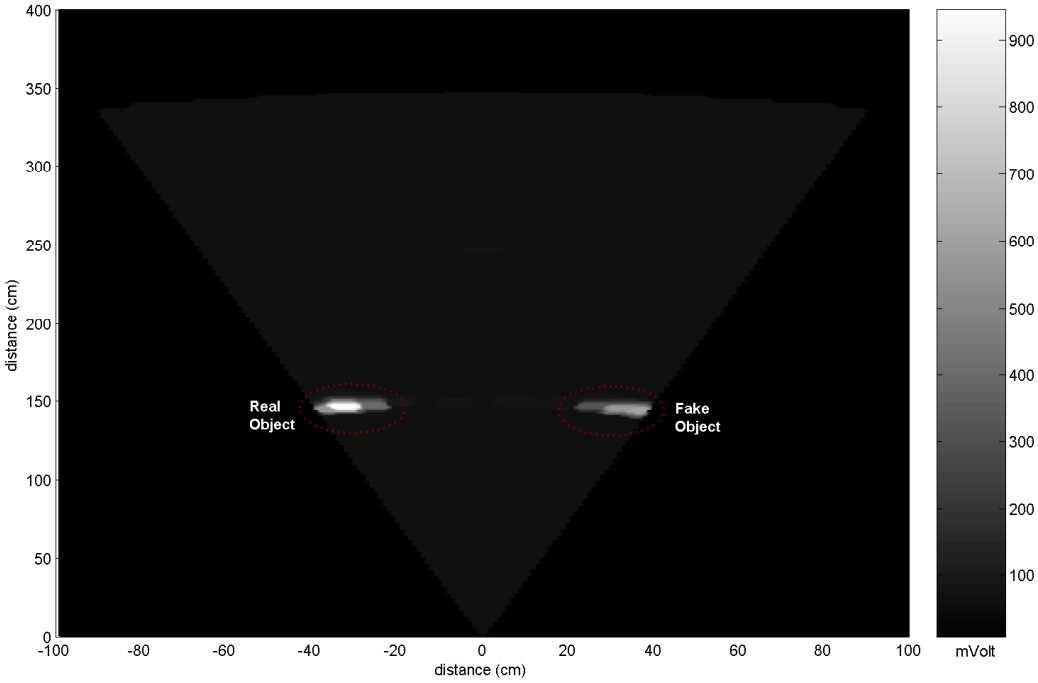

Figure 5.27: Experiment VII Result

Chapter 6

Conclusions

The developed ultrasonic phased array device is used for acoustic imaging and object detection. Although there is overlap between the techniques of radar and ultrasonic imaging, the device is not radar with sound. The radar is usually used to detect individual moving targets, but the developed device is used for detecting and separating standing objects from each other. Secondly, in radar applications the noise is mostly the electronic noise and signal processing is used to decrease noise of receiver or optimize signal-to-noise ratio. In ultrasonic imaging there are no identifiable single targets and the noise can be both electronic noise and echoes in the sidelobes of the transducer's field. For this reason, the convolved noise to the image cannot be separated always by the techniques applied in radar [4].

In order to obtain better images, the sidelobes in the directivity pattern of the system have to be suppressed. Apodization is good solution for the case in Experiment 7. The transmitter array can be driven by signals with different amplitudes. The array is not driven uniformly; the center elements are driven with the same signal but the outer elements of the transmitter array are driven more weakly. Therefore, apodization lowers the sidelobe level of the field pattern, but it also expands the main beam.

As a future work, the number elements on the transducers array can be increased and apodization can be applied. Increasing the number of elements narrows the main beam and the expanded beam by apodization can be compensated. With the combination of apodization and increased array elements, better directivity patterns can be achieved for the overall system.

6.1 Error Factors

While detecting an object, the exact place of it can be misjudged due to error factors stated below. The measured angle (θ) and the distance (r) of the object can be vary for different cases, dependent to the accuracy of the system.

The accuracy of the transmitter and receiver array is dependent to the driver circuitry and the microprocessor, since the pulse generation and phase delays are applied by an ARM based microcontroller. In such applications, where constant pulses and phase delays are needed, the microcontroller has a big disadvantage; branch prediction and pipelining. The static branch prediction scheme of the ARM based microcontroller and the pipelining in the processing unit introduce jitter[1] in the transmitted pulse. The same number of loops and if statements can be executed with different execution times and cause jitter, because of the pipelining and the branch prediction. The frequency of a single element and relative phase delays between the array elements varies due to jitter.

The microcontroller introduces errors in angular measurements, but not in distance measurements. Although, the distance of an object cannot be detected without an error in all measurements. The main reason for this false measurement is the effect of temperature to the speed of sound.

$$c_{air} = 331.3 + (0.6 \cdot T)\text{m/s}$$

where T is the temperature in degrees Celsius (°C). In this application, since highly accurate distance information is not required, the speed of sound can be taken to be constant. A temperature change of 5° introduces an error less than 1%. Although in an application requiring very accurate distance measurements, the variation in the temperature would have to be compensated for.

6.1.1 Frequency Errors

Measurements show that the frequency of the pulsed signal from the transmitter array changes between 40.4 kHz and 41 kHz where working frequency of the system is 40.8 kHz.

[1] *Jitter* is the unwanted variation of the signal's interval between successive pulses, the frequency or phase of successive cycles.

For observing the error introduced by the frequency shift, it is assumed that the array is focused to $10°(\theta = 80°)$ and there is no phase and placement errors. By using the Equation 2.16:

$$\beta = -kd\cos\theta$$

and

$$c = \lambda \cdot f$$

the error introduced by frequency shift can be calculated as below:

$$\beta = -\frac{2\pi}{\lambda} d\cos\theta$$
$$\beta = -\frac{2\pi f}{c} d\cos\theta$$

$$\text{For } f = 40.8\text{kHz} \rightarrow \theta = 10°$$
$$\text{For } f = 40.4\text{kHz} \rightarrow \theta = 10.1°$$
$$\text{For } f = 41\text{kHz} \rightarrow \theta = 9.95°$$

$$\text{Frequency Error} = +1\% \text{ to } -0.5\%$$

6.1.2 Phase Errors

It is measured that the microcontroller introduces $\pm 2°$ phase shift. With a similar approach to frequency errors, the phase errors can be calculated with the same equation:

$$\beta = -kd\cos\theta$$

By assume that the array is focused to $10°(\theta = 80°)$ and there is no frequency and placement errors.

$$\text{For } \beta = 99° \rightarrow \theta = 10°$$
$$\text{For } \beta = 101° \rightarrow \theta = 9.8°$$
$$\text{For } \beta = 97° \rightarrow \theta = 10.2°$$

$$\text{Phase Error} = \pm 2\%$$

6.1.3 Placement Errors

Since the placements of the transducers are done by hand, there is a placement error of 0.15mm. By assuming that the array is focused to $10°(\theta = 80°)$ and there is no frequency and phase errors, and using Equation 2.16 again:

$$\begin{aligned}
\text{For} \quad d &= 2.11\lambda \quad \rightarrow \quad \theta = 10° \\
\text{For} \quad d &= 2.11\lambda + 0.15\text{mm} \quad \rightarrow \quad \theta = 9.82° \\
\text{For} \quad d &= 2.11\lambda - 0.15\text{mm} \quad \rightarrow \quad \theta = 10.18°
\end{aligned}$$

$$\text{Placement Error} = \pm 1.8\%$$

$$\boxed{\text{Total Angular Error} = +4.8\% \text{ to } -4.3\%}$$

Bibliography

[1] K. Higuchi, K. Suzuki, and H. Tanigawa, "Ultrasonic phased array transducer for acoustic imaging in air," *IEEE Ultrasonics Symposium*, pp. 559–562, 1986.

[2] C. Wykes, F. Nagi, and P. Webb, "Ultrasound imaging in air," *International Conference on Acoustic Sensing and Imaging*, pp. 77–81, 1993.

[3] M. Moebus and A. M. Zoubir, "Three-dimensional ultrasound imaging in air using a 2d array on a fixed platform," *IEEE International Conference on Acoustics, Speech and Signal Processing*, vol. 2, pp. II–961–II–964, 2007.

[4] T. A. Shoup and J. Hart, "Ultrasounic imaging systems," *IEEE Ultrasonics Symposium*, vol. 2, pp. 863–871, 1989.

[5] J. Richardson, K. Marsh, J. Schoenwald, and J. Martin, "Acoustic imaging of solid objects in air using a vall set of transducers," *IEEE Ultrasonics Symposium*, pp. 831–836, 1984.

[6] O. Lahav and D. Mioduser, "A blind persons cognitive mapping of new spaces using a haptic virtual environment," *Journal of Research in Special Educational Needs*, vol. 3, no. 3, pp. 172–177, 2003.

[7] K. Lynch, *The image of the city.* Cambridge, Ma.: MIT Press, 1960.

[8] L. Russel, "Travel path sounder," in *Proceedings Rotterdam Mobility Research Conference.* New York: Amer. Foudation for the Blind, 1965.

[9] L. Kay, "An ultrasonic sensing probe as a mobility aid for the blind," *Ultrasonics*, vol. 2, p. 53, 1964.

[10] N. Pressey, "Mowat sensor," *Focus*, vol. 3, pp. 35–39, 1977.

[11] A. Heyes, "Sonic pathfinder: a programmable guidance aid for the blind," *Electronics and Wireless World*, vol. 90, no. 1579, pp. 26–29,62, 1984.

[12] A. Dodds, J. Armstrong, and C. Shingledecker, "The nottingham obstacle detector: development and evaluation," *Journal of Visual Impairment and Blindness*, vol. 75, no. 5, pp. 203–209, 1981.

[13] S. Shoval, J. Borenstein, and Y. Koren, "Mobile robot obstacle avoidance in a computerized travel aid for the blind," *IEEE International Conference on Robotics and Automation*, vol. 3, pp. 2023–2028, 1994.

[14] T. Hoydal and J. Zelano, "An alternative mobility aid for the blind: the 'ultrasonic cane'," *IEEE Bioengineering Conference*, pp. 158–159, 1991.

[15] R. Gao and L. Chuan, "A dynamic ultrasonic ranging system as a mobility aid for the blind," *Engineering in Medicine and Biology Society, 1995. IEEE 17th Annual Conference*, vol. 2, pp. 1631–1632, 1995.

[16] D. Batarseh, T. Burcham, and G. McFadyen, "An ultrasonic ranging system for the blind," *IEEE Biomedical Engineering Conference*, pp. 411–413, 1997.

[17] X. Cai and R. Gao, "Data fusion for obstacle identification using ultrasonic sensing," *IEEE Instrumentation and Measurement Technology Conference*, vol. 2, pp. 834–838, 2000.

[18] M. Choudhury, D. Aguerrevere, and A. Barreto, "A pocket-pc based navigational aid for blind individuals," *IEEE Symposium on Virtual Environments, Human-Computer Interfaces and Measurement Systems*, pp. 43–48, 2004.

[19] N. Debnath, Z. Hailani, S. Jamaludin, and S. Aljunid, "An electronically guided walking stick for the blind," in *Proceedings of the 23rd Annual International Conference of the IEEE Engineering in Medicine and Biology Society*, vol. 2, 2001, pp. 1377–1379.

[20] S. Tachi and K. Komoria, "Guide dog robot," in *Proceedings of the 2nd International Congress on Robotics Research, Kyoto, Japan*, 1984.

[21] P. Aigner and B. McCarragher, "Shared control framework applied to a robotic aid for the blind," *IEEE Control Systems Magazine*, vol. 19, pp. 40–46, 1999.

[22] S.-J. Kang, Y. Ho, and I. H. Moon;, "Development of an intelligent guide-stick for the blind," *IEEE International Conference on Robotics and Automation*, vol. 4, pp. 3208–3213, 2001.

[23] I. Shim and J. Yoon, "A robotic cane based on interactive technology," *Industrial Electronics Society, IEEE 2002 28th Annual Conference of the*, vol. 3, pp. 2249–2254, 2002.

[24] J. Borenstein and Y. Ulrich, "The guidecane-a computerized travel aid for the active guidance of blind pedestrians," in *Proceedings IEEE International Conference on Robotics and Automation*, vol. 2, 1997, pp. 1283–1288.

[25] S. Shoval, J. Borenstein, and Y. Koren, "Navbelt and the guide-cane [obstacle-avoidance systems for the blind and visually impaired]," *IEEE Robotics and Automation Magazine*, vol. 10, no. 1, pp. 9–20, 2003.

[26] M. Strakowski, B. Kosmowski, R. Kowalik, and P. Wierzba, "An ultrasonic obstacle detector based on phase beamforming principles," *IEEE Sensors Journal*, vol. 6, no. 1, pp. 179–186, 2006.

[27] G. of Telecommunication Terms, Federal Standard 1037C, 1996.

[28] R. Mailloux, *Phased Array Antenna Handbood*, 2nd ed. Artech House, 2005.

[29] C. A. Balanis, *Antenna Theory*, 3rd ed. Wiley-Interscience, 1997, ch. Arrays: Linear, Planar, and Circular, pp. 283–320.

[30] K. Yee, "Numerical solution of initial boundary value problems involving maxwell's equations in isotropic media," *IEEE Transactions on Antennas and Propagation*, vol. 14, no. 3, pp. 302–307, 1966.

[31] A. Taflove, *Advances in computational electrodynamics: the finite-difference time-domain method*. Boston: Artech House, 1998.

[32] A. Taflove, "Review of the formulation and applications of the finite-difference time-domain method for numerical modeling of electromagnetic wave interactions with arbitrary structures," *Wave Motion*, vol. 10, pp. 547–582, 1988.

[33] J. Berenger, "A perfectly matched layer for the absorption of electromagnetic waves," *Journal of Computational Physics*, vol. 114, no. 2, pp. 185–200, 1994.

[34] K. Shlager and J. Schneider, "A selective survey of the finite-difference time-domain literature," *IEEE Antennas and Propagation Magazine*, vol. 37, no. 4, pp. 39–57, 1995.

[35] T. Miyashita, "Sonic crystals and sonic wave-guides," *Measurement Science and Technology*, vol. 16, pp. R47–R63, 2005.

[36] A. Taflove and S. C. Hagness, *Computational electrodynamics: the finite-difference time-domain method*, 2nd ed. Boston: Artech House, 2000.

[37] P. Pedersen and A. Nadkami, "Optimization of an array based pulse-echo system for identification of reflector geometry," *IEEE Ultrasonics Symposium*, vol. 2, pp. 1050–1053, 2004.

[38] T.-O. Hoydal, "Ultrasonic cane for the blind," Department of Electrical Engineering, New Jersey Institute of Technology," Engineering Senior Design Projects to Aid the Disabled, 1990.

[39] N. Debnath, J. Thangiah, S. Pararasaingam, and S. Aljunid, "A mobility aid for the blind with discrete distance indicator and hanging object detection," *IEEE Region 10 Conference TENCON*, vol. 4, pp. 664–667, 2004.

[40] M. O. Lammers, M. Schotten, and W. W. L. Au, "The spatial context of free-ranging hawaiian spinner dolphins (stenella longirostris) producing acoustic signals," *Acoustical Society of America*, vol. 119, no. 2, pp. 1244–1250, 2006.

[41] *SRF04 - Ultra-Sonic Ranger*, Devantech, 2003.

Appendix A

Directivity Patterns For Different Angles

The following figures show the directivity patterns of transmitter array, receiver array, and overall system, respectively. The dashed red lines in the figures represent the theoretical calculations. The blue lines in the figures are plotted according to directivity measurements, where the measurement setup is described in Chapter 5.

Phase differences between the elements for specific focusing angles are calculated with the Equation 2.16:

$$\beta \;=\; -kd\cos\theta$$

For each focusing angle the following phase delays are achieved:

FA	0°	2.5°	5°	7.5°	10°	12.5°	15°
PDTA	0°	-33°	-66°	-99°	-132°	-164°	-196°
PDRA	0°	-80.7°	-161°	-241°	-321°	-400°	-479°

Table A.1: Phase delays between the array elements

where

FA means "Focusing angles",

PDTA means "Phase delays between the elements of transmitter array",

PDRA means "Phase delays between the elements of receiver array".

For negative focusing angles, the directivity patterns are completely symmetrical with the positive ones. Also the phase delays are same except the minus sign.

Focused to 0°

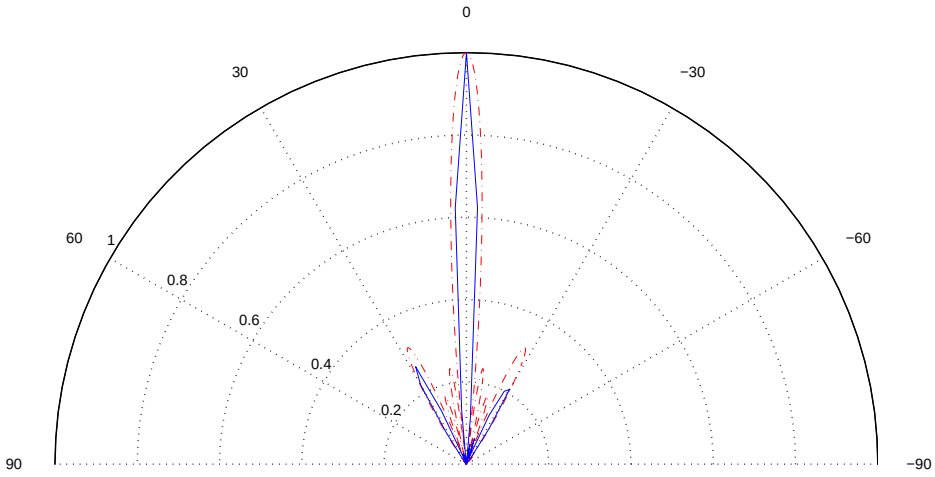

Figure A.1: Directivity Pattern of Transmitter Array (for 0°)

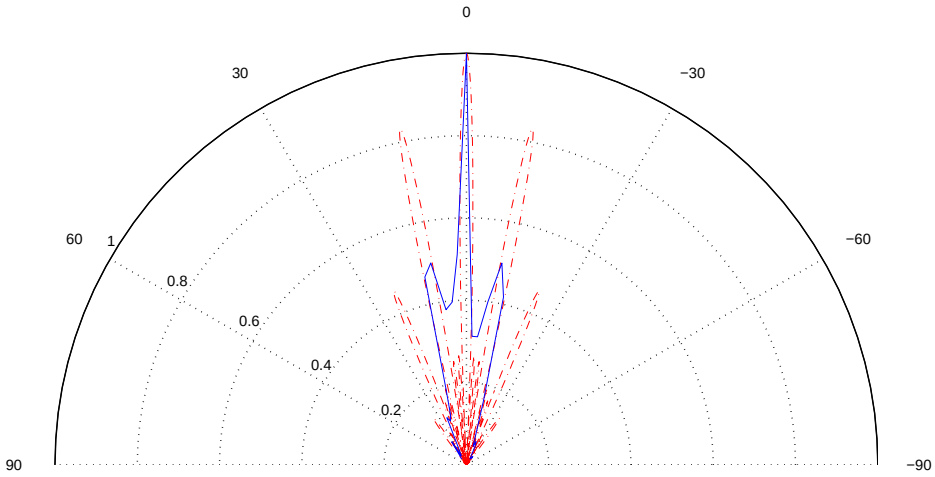

Figure A.2: Directivity Pattern of Receiver Array (for 0°)

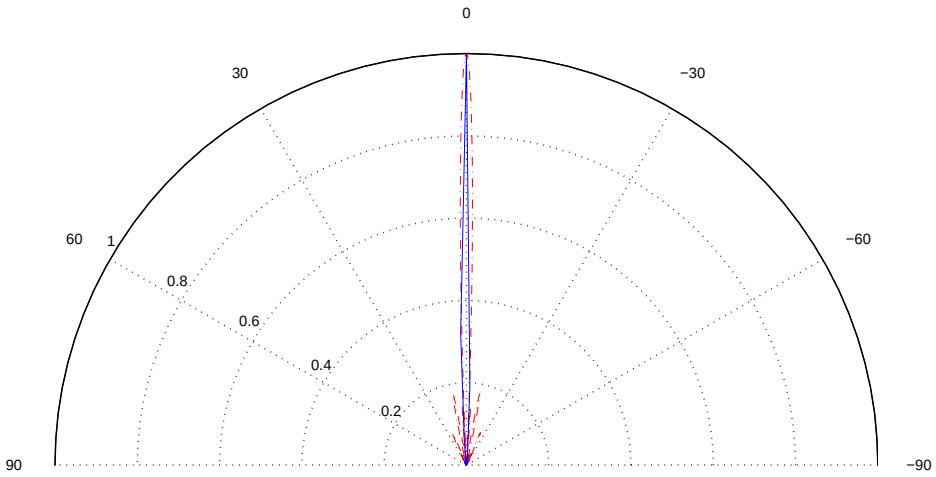

Figure A.3: Directivity Pattern of Overall System (for 0°)

Focused to 2.5°

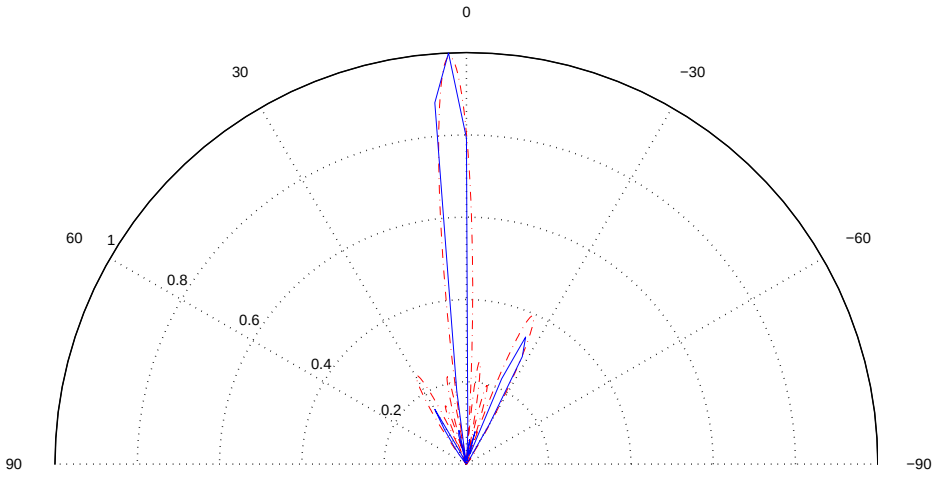

Figure A.4: Directivity Pattern of Transmitter Array (for 2.5°)

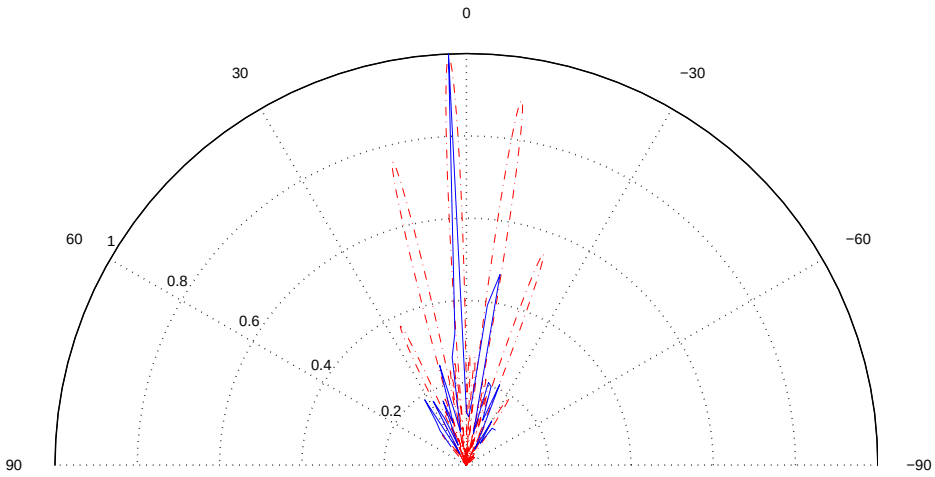

Figure A.5: Directivity Pattern of Receiver Array (for 2.5°)

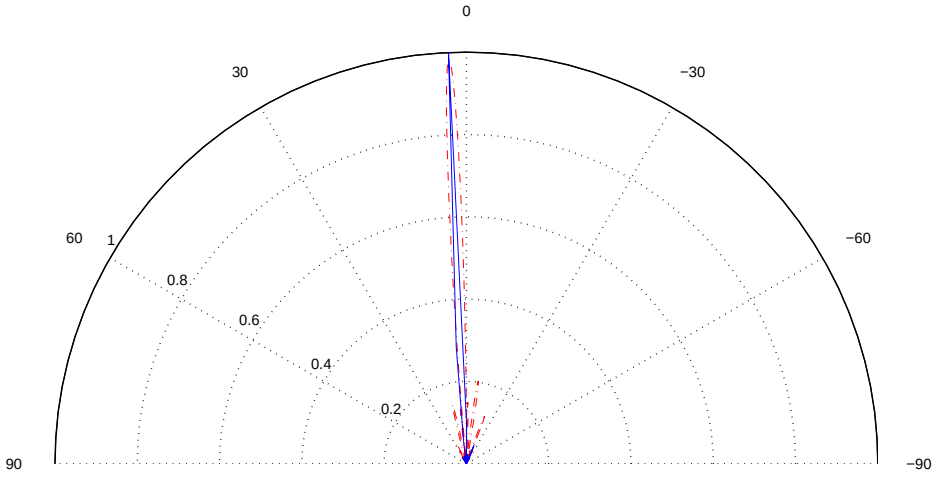

Figure A.6: Directivity Pattern of Overall System (for 2.5°)

Focused to 5°

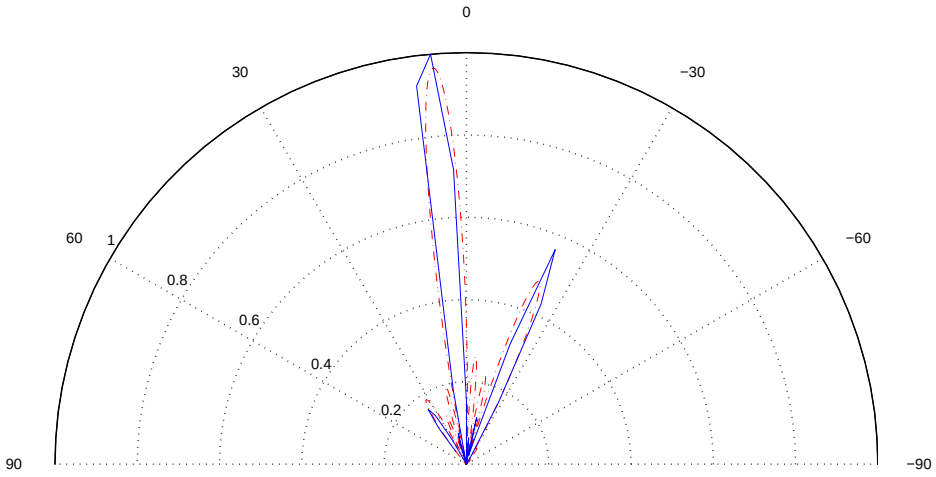

Figure A.7: Directivity Pattern of Transmitter Array (for 5°)

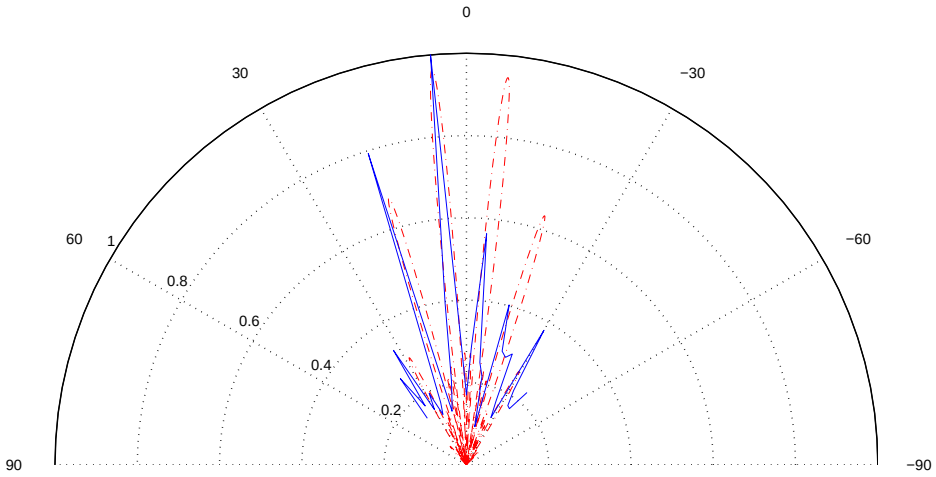

Figure A.8: Directivity Pattern of Receiver Array (for 5°)

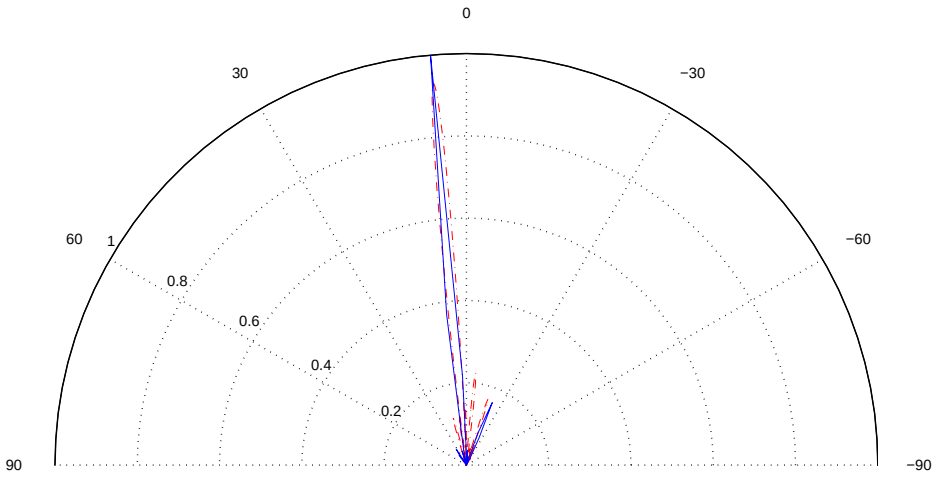

Figure A.9: Directivity Pattern of Overall System (for 5°)

Focused to 7.5°

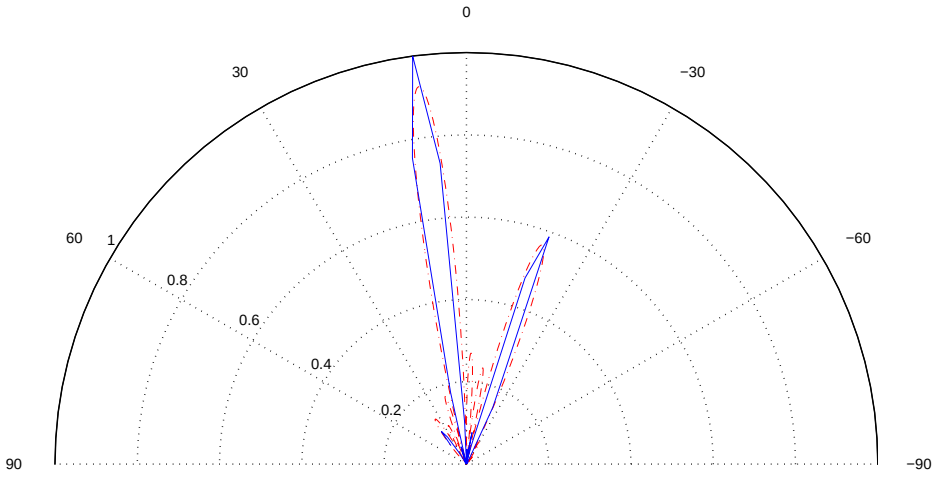

Figure A.10: Directivity Pattern of Transmitter Array (for 7.5°)

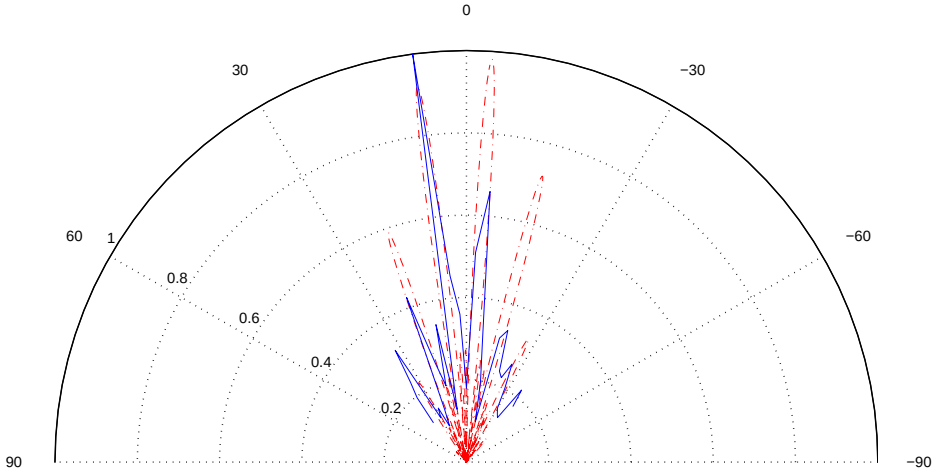

Figure A.11: Directivity Pattern of Receiver Array (for 7.5°)

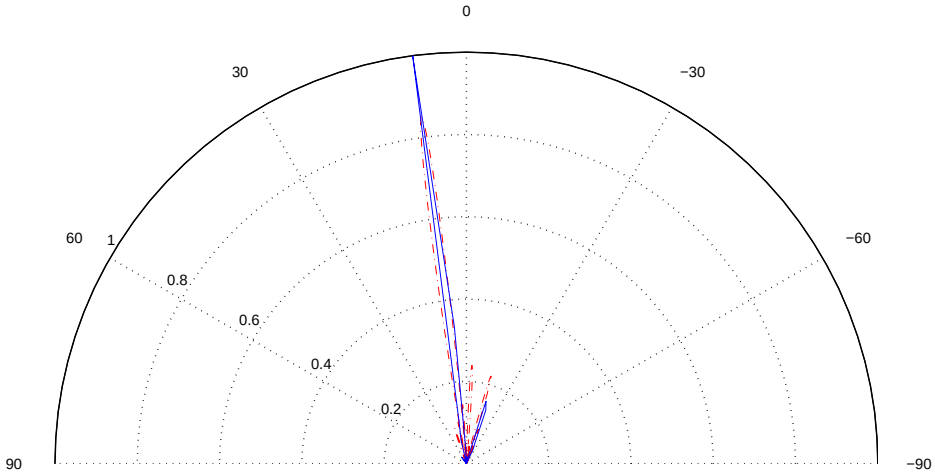

Figure A.12: Directivity Pattern of Overall System (for 7.5°)

Focused to 10°

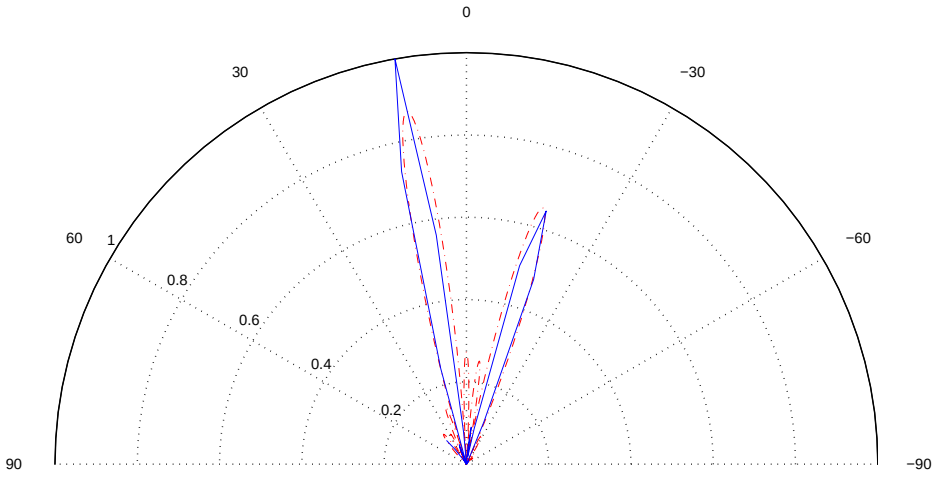

Figure A.13: Directivity Pattern of Transmitter Array (for 10°)

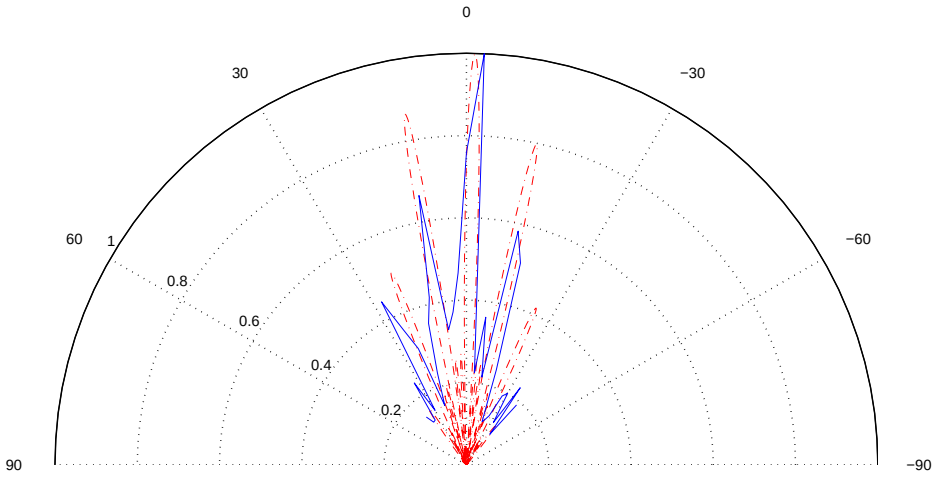

Figure A.14: Directivity Pattern of Receiver Array (for 10°)

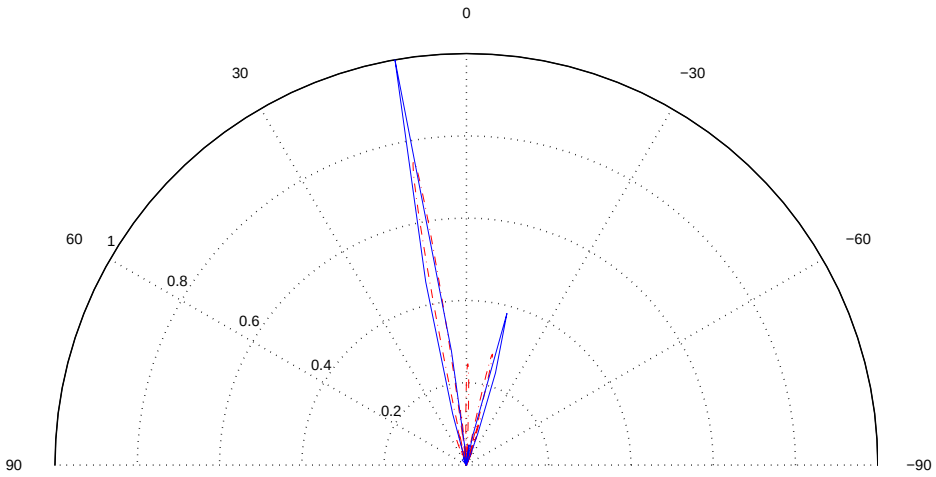

Figure A.15: Directivity Pattern of Overall System (for 10°)

Focused to 12.5°

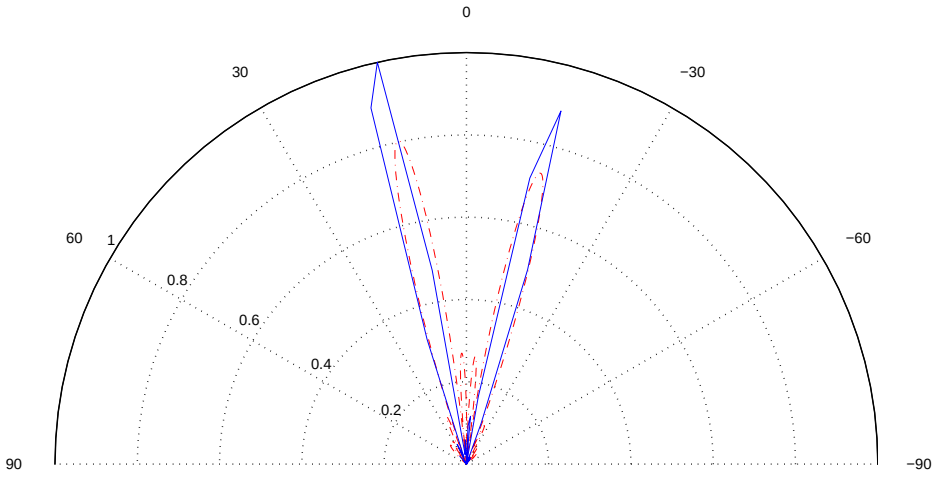

Figure A.16: Directivity Pattern of Transmitter Array (for 12.5°)

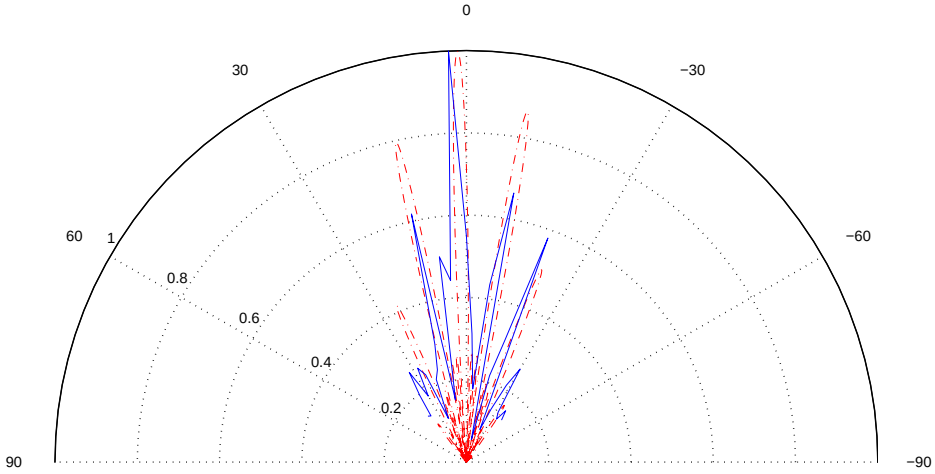

Figure A.17: Directivity Pattern of Receiver Array (for 12.5°)

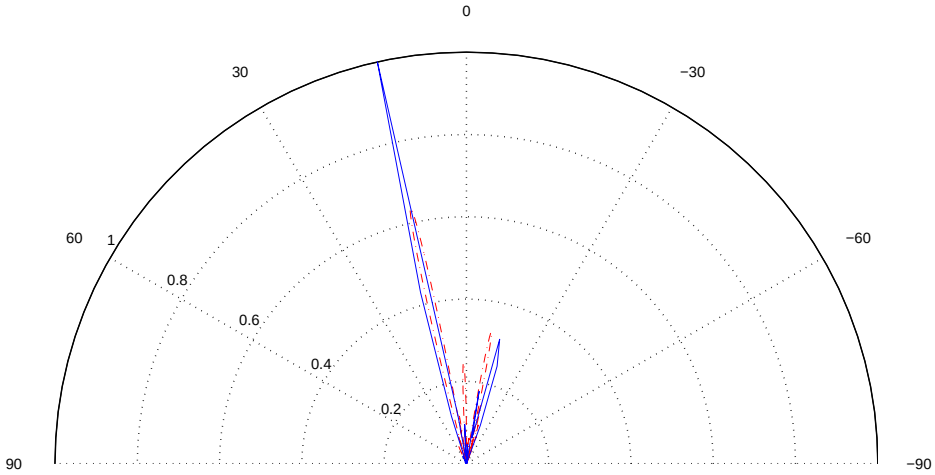

Figure A.18: Directivity Pattern of Overall System (for 12.5°)

Focused to 15°

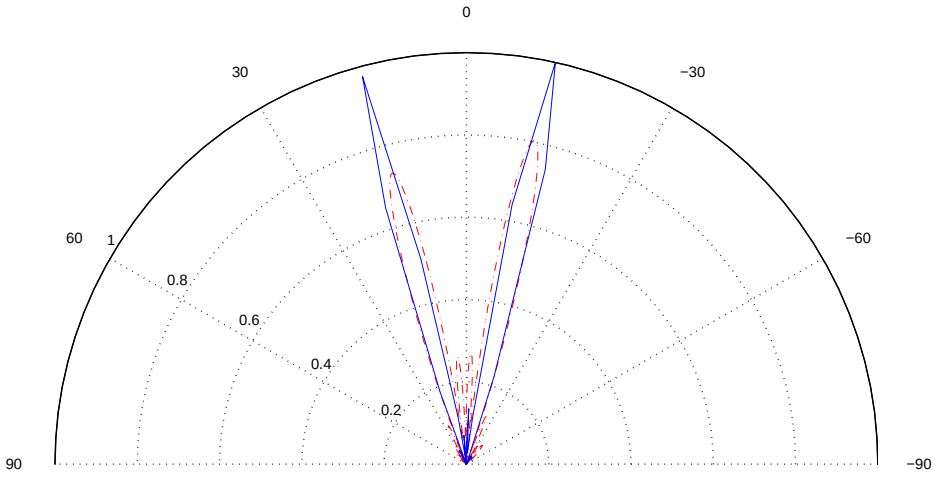

Figure A.19: Directivity Pattern of Transmitter Array (for 15°)

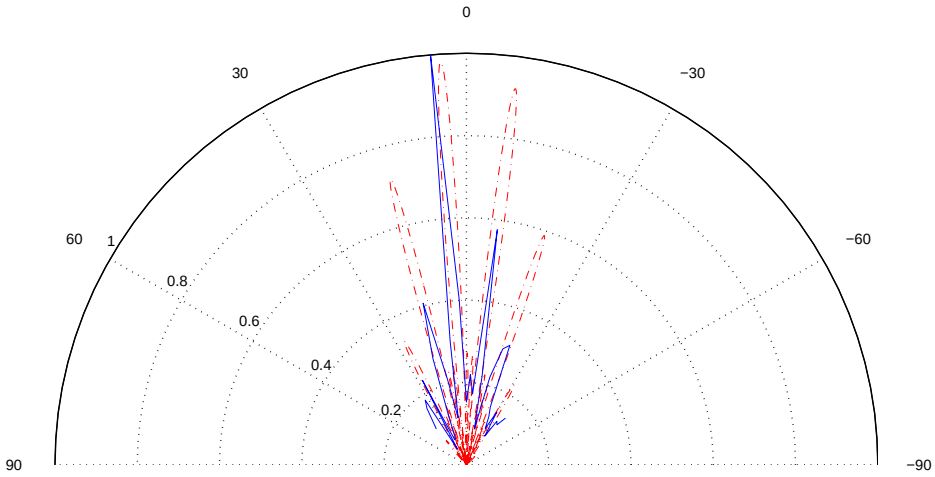

Figure A.20: Directivity Pattern of Receiver Array (for 15°)

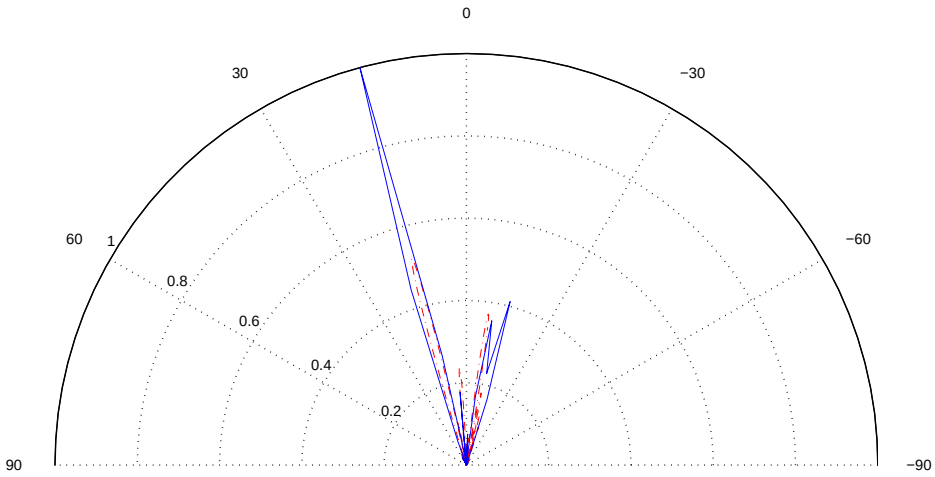

Figure A.21: Directivity Pattern of Overall System (for 15°)

Note: In the theoretical calculations all of the array elements are assumed to have the same angle with the focusing angle for far-field observations, but all of the transducers are placed with a different angle relative to a specific point in the space. In this case the receiver array is placed with a spacing of 5.14 λ and it causes the assumption to fail. Therefore, for some focusing angles the theoretical calculations and measurements do not match completely. In some of the figures the side lobes are smaller and they are displaced.

Appendix B

Receive Beam Forming

The ultrasonic phased array device receives the echo from environment. The received data is transfered to the computer via serial port. The coming data from serial port is saved into a text file. Before starting receive beam forming, Matlab reads the text file.

```
fid = fopen('Received_Data.txt','r');
Received_Data = fread(fid);
```

The received data is a sampled with a 12-bit ADC, for this reason the consecutive two bytes are added and the 12-bit data is achieved.

```
[size_RD temp] = size(Received_Data);


for n = 1:(size_RD/2)
   Reformed_Data((n) = Received_Data(2*n) + Received_Data(2*n-1)*256;
end
```

After reforming the received data, it is interpolated up in order to achieve a better overlap while implementing the phase differences. The sampling rate is 1.675 μsec, but a phase difference of 5.5 μsec is needed. Since 1.675 is not a multiple of 5.5, the received data is interpolated to achieve a 1.375 μsec sampling rate ($4 \times 1.375 = 5.5$).

```
temp_Data = interp(Reformed_Data,39);
Interpolated_Data = downsample(temp_Data,32);
```

The received data from the device includes the sampled data from RX0, RX1, RX2, and RX3, respectively (RX0 is the first element o receiver array). The received data from each transducer is separated as below, before implementing required phase differences.

```
[temp size_ID] = size(Interpolated_Data);


for n = 1:(size_ID/4)
  RX0(n) = Interpolated_Data(n);
  RX1(n) = Interpolated_Data((size_ID/4)+n);
  RX2(n) = Interpolated_Data(2*(size_ID/4)+n);
  RX3(n) = Interpolated_Data(3*(size_ID/4)+n);
end
```

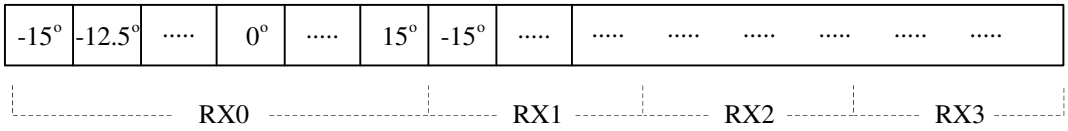

Figure B.1: Received data

After separating the data coming from each transducer, 13 different arrays are formed for 13 different focusing angles. The RX0 includes the data coming from 13 different focusing angles between -15° to 15°, which are increasing with a rate of 2.5°. For example, when calculating the returning echo from -15°, the phase difference of 33 μsec is needed (33/1.375 = 24). For this reason, the data received from -15° for each transducer is added up by shifting the next transducers data by 24.

```
[temp size_RX] = size(RX0);


m15deg(1:size_RX/13) = RX0(1:size_RX/13);
m15deg(25:24+size_RX/13) = m15deg(25:24+size_RX/13) + RX1(1:size_RX/13);
m15deg(49:48+size_RX/13) = m15deg(49:48+size_RX/13) + RX2(1:size_RX/13);
m15deg(73:72+size_RX/13) = m15deg(73:72+size_RX/13) + RX3(1:size_RX/13);
```

By this way, the returning echo received by the receiver array from the -15° is formed by applying necessary phase differences between the array elements.

After constructing the arrays for each angles, the data is switched to cartesian coordinates from polar coordinates, for plotting. x and y are calculated for cartesian coordinates rather than r and θ. The 344000 in the formulations is the speed of sound in mm/sec and some offset is added for y axis in order to center the plot.

```
[temp size_M15d] = size(m15deg);
time_step_size = 1.375e-6;


for theta = -15:2.5:15
  for m = 1:size_M15d
   x = 1 + round(m*time_step_size*344000*cosd(theta));
   y = offset + round(m*time_step_size*344000*sind(theta));
   if (theta == -15)
    Acoustic_image(x,y) = m15deg(m);
   end
      .
      .
      .
   if (theta == 15)
    Acoustic_image(x,y) = p15deg(m);
   end
  end
end
```

After constructing the acoustic image in cartesian coordinates the missing elements of the matrix is interpolated and the final figure is plotted.